9-11-2008

Footprint Modeling and Connectivity Analysis for Wireless Sensor Networks

Changfei Chen
University of Vermont

FOOTPRINT MODELING AND CONNECTIVITY ANALYSIS FOR WIRELESS SENSOR NETWORKS

A Thesis Presented

by

Changfei Chen

to

The Faculty of the Graduate College

of

The University of Vermont

In Partial Fulfillment of the Requirements
for the Degree of Master of Science
Specializing in Electrical Engineering

October, 2008

Accepted by the Faculty of the Graduate College, The University of Vermont, in partial fulfillment of the requirements for the degree of Master of Science, specializing in Electrical Engineering.

Thesis Examination Committee:

_____ **Advisor**
Jeff Frolik, Ph.D.

_____
Paul Hines, Ph.D.

_____ **Chairperson**
Jeff Dinitz, Ph. D.

_____ **Vice President for Research**
Frances E. Carr, Ph. D **and Dean of Graduate Studies**

Date: June 26, 2008

ABSTRACT

A wireless sensor network is a network consisting of spatially distributed, sometime-autonomous sensors, communicating wirelessly to cooperatively achieve some task. For example, a wireless sensor network may be used for habitat monitoring to ascertain the environment's temperature, pressure, humidity, etc. In order for a wireless sensor network to provide such data, one needs to ensure there is connectivity between nodes. That is, nodes can communicate to exchange information. To analyze connectivity between sensors, the radio communication range of each sensor, also called the communication footprint, needs to be known. To date, the models used to analyze a sensor's radio communication footprint have been overly simplistic (i.e., isotropic) and thus yield results not found in practice. Footprints are highly dependent on the deployment environments, which are typically heterogeneous and non-isotropic in structure.

In this work, a 'weak-monotonicity' (W-M) model is leveraged to represent a footprint's non-isotropic behavior. The work also considers the heterogeneity of the environment through the use of the log-normal shadowing model. In particular, the usable percentage of the W-M footprint (the area where the power exceeds the receiver threshold) in such environments is considered through analysis and simulation. We then develop an enhanced footprint model which overlays multiple W-M patterns and use this method to represent experimental propagation data. The work also considers the use of graph theory methods to analyze the connectivity of randomly deployed networks in non-homogeneous, non-isotropic environments.

CITATION

Material from this thesis has been published in the following form:

C. Chen and J. Frolik, *Improved footprint modeling for wireless sensor networks*, IEEE Int. Symposium on Antennas and Propagation, San Diego, CA, July 5-12, 2008.

ACKNOWLEDGEMENTS

I would like to thank the Academy, my parents, Dr. Jeff Frolik for his patient guidance to all my research work, my committee for their valuable suggestions to my work, and all my friends here at UVM, in Paris and my home city, Shanghai, China. During the past two years at UVM, all of you have always been supporting me, no matter where you are. Even though some of you are thousands of miles away from me, you still cared about me and helped me a lot. I want to thank my parents here again, since that as your only child, I am sorry for being so far away from you. Your love are always an important part in my life. Without you, none of this could ever been done.

Thank you so much.

-Changfei Chen

TABLE OF CONTENTS

Page

LIST OF TABLES

Table page

LIST OF FIGURES

Figure Page

CHAPTER 1

INTRODUCTION

1.1 Motivation

Wireless sensor networks (WSN) consist of spatially distributed autonomous sensors, communicating wirelessly in order to cooperatively achieve some task, such as environment monitoring, structural health monitoring or military surveillance [1]. For example, [2] presented a wireless sensor network used for habitat monitoring on Great Duck Island, Maine, in which temperature, pressure, humidity data was collected to monitor the behavior of birds with the change of weather. In order to support such applications, one finds that sensor nodes need to be deployed (sometimes randomly) over a large area. As such, the connectivity of the network, which pertains to the wireless communication between nodes, may not be known *a priori*. To better understand connectivity among nodes, one must consider the footprint of individual sensors, where the footprint is defined to be the effective wireless communication range as a function of direction.

In most existing connectivity analyses, the footprint used is the disk model [18] (Fig. 1) for which the communication range of each sensor is constant in all directions. Even though the disk model simplifies the calculation of the network, it is far and away from a realistic representation. Footprints highly depend on the environment the device is deployed in. These environments are typically heterogeneous and non-isotropic in

structure. In this work, we will research an improved footprint model in order to enable more realistic simulation and analytical results of network connectivity.

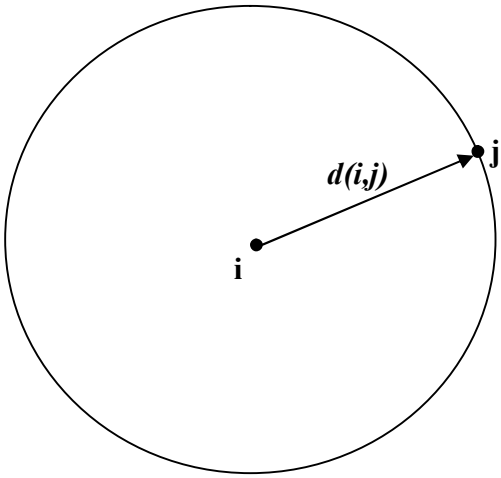

Figure 1. Uniform Disc Model

1.2 Non-Isotropic Phenomena

In order to predict and analyze the wireless signal strength at a certain location, two kinds of phenomena need to be considered: Large-scale and small-scale propagation effects. Large-scale effects describe the change of the signal strength over large distance scales. For example, on average the signal strength received decreases as the distance between the transmitter and receiver becomes larger. Small-scale effects, on the other hand, describe signal fluctuations under the influence of small changes in distance (or time). Due to these small-scale effects, the received signal strength may change significantly even for the same transmitter-receiver (T-R) distance. The surrounding environment (i.e., the obstacles around the transmitter and receiver) is the main influence

on signal propagation. Such objects (e.g., trees) can attenuate the radio signal, a phenomenon referred to shadowing. Other objects (e.g., buildings) will reflect signals creating a multipath fading environment. Signals may also bend around large objects by diffraction. These phenomena contribute to create a non-isotropic signal strength profile. The log-normal shadowing model, which will be introduced more in Section 2.2.2, uses a random variable to describe this heterogeneous property.

1.3 Link Quality Model

Energy models show the relationship between energy and transmission distance. However, if we want to model the footprints, we also need to know the boundary of the communication range. That is, the range within which a signal is sufficiently strong to meet the needs of the application. One of the existing models that provides the boundary of the communication range is the 'Link quality model' [12]. In that work the link quality was assumed to be 100% within some range and 0% for the outside part. This is effectively a unit disc representation with an idealized environment and communication link. The link quality should be expected to change gradually with distance. [10], [15] included a transition region, located between the good and bad region. As seen in Fig. 2, the transition region is from distance *D1* to *D2*. Within this transition region, the link quality is linearly decreasing with the distance. Even though the transition region improved the representative of link quality model, it still over simplified the footprints making itself far away from the real footprint.

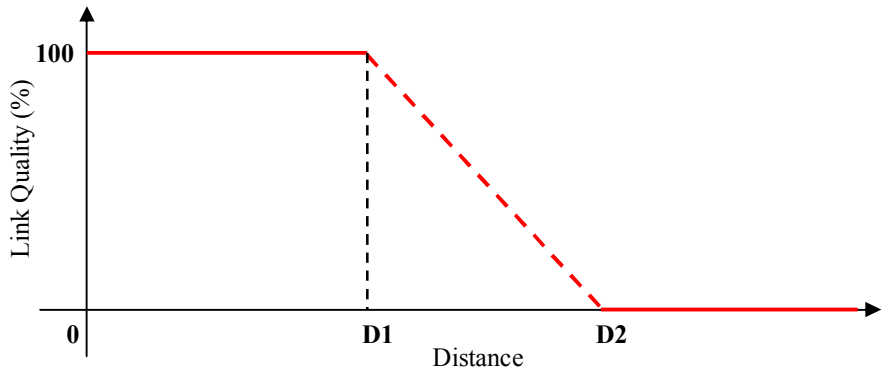

Figure 2. Link quality model with transition region [D1, D2]

As noted earlier, due to small-scale effects, the received signal strength may vary as a function of location even if the T-R distance is the same. In short, even if we have found a realistic footprint, the coverage within the footprint can not be assumed to be 100%. Some environments may be quite complex in structure and thus the signals may be very low in certain pockets. Considering that, we need to analyze the percentage of the footprint area with guaranteed connection, that is, its *usability*.

1.4 Contributions

Presently footprint and link quality models utilized in wireless sensor network research are overly ideal. In this work, we present models to better represent the non-isotropic and non-homogeneous propagation environments where sensor networks may be deployed. Specifically, the contributions of this work are:

1. A ‘weak-monotonicity’ (W-M) model is leveraged to represent a footprint’s non-isotropic behavior. In addition, the usability of the W-M footprint in a log-normal shadowing propagation environment is considered through analysis and simulation.
2. An enhanced footprint model which overlays multiple W-M patterns is developed. We illustrate that real data can be represented by our new overlapping model and thus provide more realistic footprints of sensors.
3. We analyze the connectivity of wireless sensor networks randomly deployed in non-homogeneous environments to find the weakest link which can ensure connectivity of the network. This information can assist in ascertaining the robustness of the network’s connectivity.

These contributions will help the analyses of connectivity in wireless sensor networks and thus enhance the reliability, robustness and lifetime of these systems.

1.5 Outline

Chapter 1 presented an introduction, the motivation and the main contributions of this work. The remainder of this thesis is organized as follows. Chapter 2 introduces related work and model. In particular, the ‘Weak-Monotonicity’ (W-M) model is presented. Chapter 3 will focus on usability analysis of the W-M model. Real data collection and analysis will be discussed in Chapter 4. The connectivity analysis of the network will discussed at Chapter 5. Finally, our conclusion for the thesis along with the future work is presented in Chapter 6.

CHAPTER 2

RELATED WORK AND MODELS

2.1 Introduction

In this chapter, we will introduce the Weak-Monotonicity footprint model. The energy and log-normal shadowing models which are related to our work will also be discussed. Finally, earlier usability results, which did not take into account a non-isotropic footprint, will be presented.

2.2 Related Footprint Work

In [3], D'Souza, et al proved that with some local geometric θ-constraints, the connectivity of the networks can be confirmed, which means any two nodes in the network can be able to communication with each other either directly or through other nodes. The concept of 'θ-constraints' comes from Adaptive Topology Power Control (ATPC), which is a local geometry algorithm which constructs a graph with only a single parameter, 'θ', the angle between two continuous neighbors. We illustrate this concept in Fig. 3. Node *T* is the transmitting device. Five other nodes, *R1, R2,..., R5*, are able to communicate with and become its neighbors. Successive neighbors construct angles, $\theta 1, \theta 2, \ldots, \theta 5$, between each other. If we constrain the angles to some value, for example π, and $\theta 1, \theta 2, \ldots, \theta 5$ are smaller than π, we can then say that the 'π-constraints' is satisfied.

Two footprint models, 'Bounded Eccentricity' (B-E) and 'Weak-Monotonicity' (W-M), were also proposed in [3] to address the shortcomings of the traditional disk model. The B-E model limits footprint coverage to a smaller disc area, so we can expect more reliable links within the footprint. The W-M model is not constrained to the assumption of isotropic coverage. The following sections describe these two footprint models.

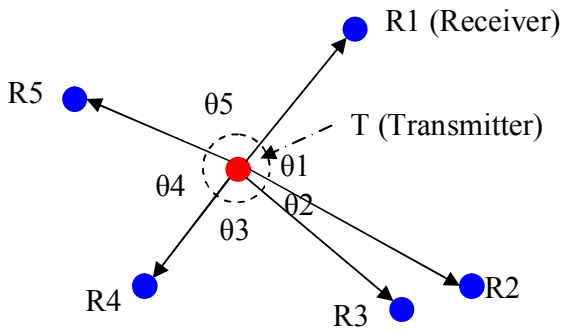

Figure 3. Definition of parameter θ in a graph

2.2.1 Bounded Eccentricity Model

In the 'Bounded Eccentricity' model (Fig. 4), each sensor contains a uniform disc whose radius is some constant fraction of the distance to the farthest node which can be communicated with. The sensor will then have guaranteed connectivity with all nodes in this smaller disc. In Fig. 4, let j be the farthest node from node i that can be communicated with and let the distance between i and j be given by $d(i,j)$. This distance, d, between nodes is also referred to as the T-R (transmitter-receiver) distance. Then 'eccentricity', a, is the smallest number to ensure that any node, k, with the property: $d(i,k) \le d(i,j)/a$, is connected to i. Since connectivity is guaranteed within

the disc of radius $|d(i,j)/a|$, this footprint is said to provide 100% usability. Usability will be discussed further in Section 2.5.

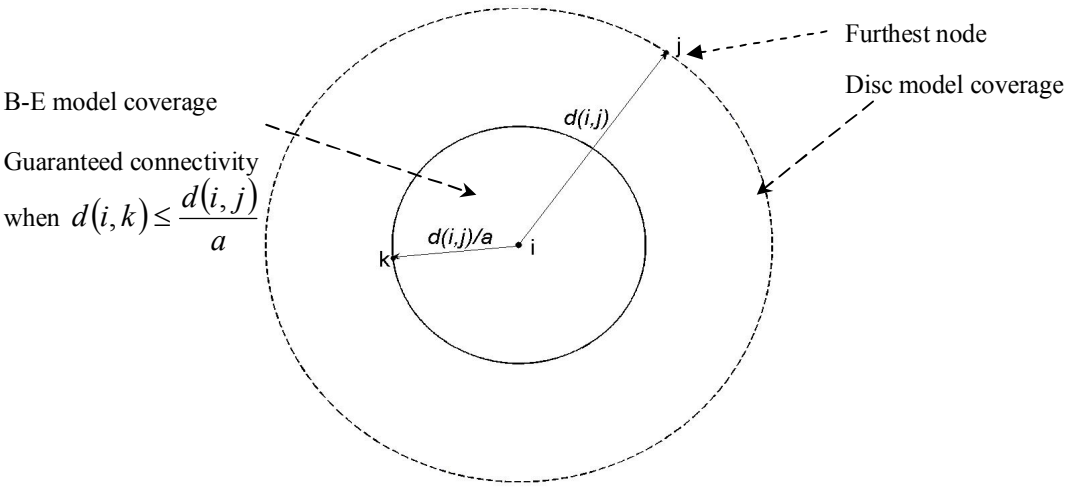

Figure 4. 'Bounded Eccentricity' Model

In the uniform disc model, all nodes are assumed to have the same footprint. In the bounded eccentricity model, however, node footprints are dependent on the longest viable communication link which is therefore dependent on node location and local environment. As such, each node's footprint (while circular) will have different radii. However, the B-E model is still a disc model with a footprint that is isotropic, and thus far away from a realistic representation. Moreover, as we look into the model, we find that we must first know the connectivity between the nodes before determining the eccentricity, *a*, of the nodes in a network. As such this model is suitable for understanding the behavior of existing networks, but not for analyzing potential connectivity of networks prior to deployment. We also note that this model is overly

conservative, since there will be nodes outside the disc for which there will be connectivity.

2.2.2 Weak-Monotonicity (W-M) Model

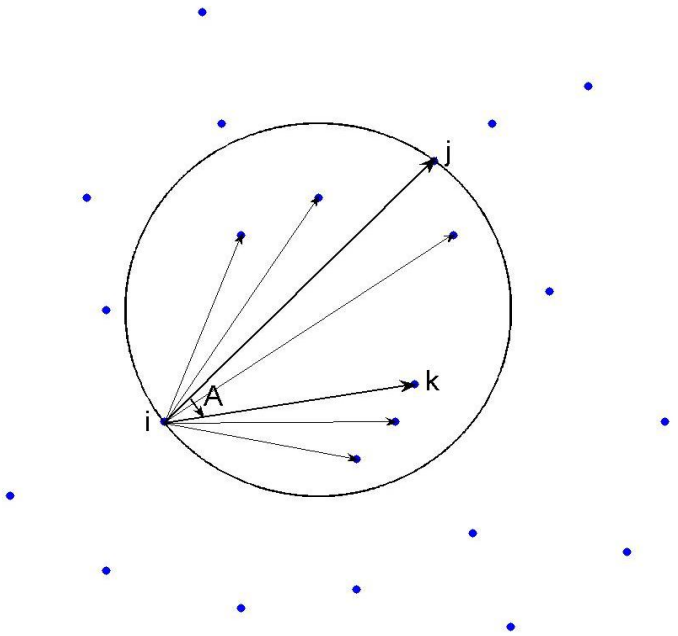

Figure 5. 'Weak-Monotonicity' Model

The name 'Weak-monotonicity' comes from 'Monotonicity', which describes the properties of the traditional disc model. In the disc model, the signal strengths are same in all directions (i.e. for all angles), so the communication range is said to be monotonic. If node *i* is connected to node *j,* then *i* will be connected to any node *k* with property $d(i,k) \le d(i,j)$. However, in the W-M model, see Fig. 5, any node, that *i* is connected to, should have the property $d(i,k) \le \cos(A) \cdot d(i,j)$, where $A = \angle jik$. Communication links are dependent on direction, thus the monotonicity is weaker. The footprint of the each

sensor in the W-M model is therefore a circle with the sensor itself on the boundary and diameter of the distance from the sensor to its farthest connected neighbor. Within the boundary, the usability is assumed to be 100%. In addition, links are assumed to be symmetric in the model.

The W-M model has fewer restrictions than the disc model in that it is not isotropic. In fact, it is restricted to a half plane. However this model also does not take into account the variability of environment and resulting propagation loss, all of which contribute to the node's actual footprint. In [3], the W-M model was assumed to have 100% connectivity within the circle range, but in practice, some areas may not be covered. So in order to better represent the practical case, we should add some variances to the coverage provided by the model. In this work, the log-normal shadowing propagation model is applied to the W-M model to improve the existing constraints of the model.

Moreover, [3] analyzed and proved the connectivity by the W-M model, when certain θ-constraints were satisfied. In our work, more detailed information about W-M model is given, for example, footprint usability compared to earlier results derived for the unit disc model. In addition, Chapter 4 describes results of using the W-M model to represent empirical data, which brings the analysis of the new model to a more practical level.

2.3 Log-Normal Shadowing Model

The average power of received signal, by large-scale propagation effects, decreases exponentially with T-R distance. For example, in free-space the power decays with

distance squared. In general, the average large-scale loss at T-R distance, d, can be represented as:

$$\overline{PL}(d) \propto \left(\frac{d}{d_0}\right)^n \tag{2.1}$$

or

$$\overline{PL}(d)\Big|_{dB} = \overline{PL}(d_0)\Big|_{dB} + 10n\log\left(\frac{d}{d_0}\right) \tag{2.2}$$

where $\overline{PL}$ is the average path-loss, which means the reduction in power density of an electromagnetic wave as it propagates through space; d_0 is a reference distance; n is the path loss exponent, the value of which depends on the communication environment.

Obviously, the log-normal model ignores the non-isotropic property of the environment. In order to overcome the shortcomings of the log-normal model, some improved models have been developed, among which is log-normal shadowing model. This model was developed for mobile communication systems, but has also been used for wireless sensor networks [4 - 7]. The model uses a shadowing component X_σ, which is a zero-mean, Gaussian random variable with standard deviation σ dB, to model the non-homogeneous nature of the propagation environment.

$$PL(d)\Big|_{dB} = \overline{PL}(d_0)\Big|_{dB} + 10n \cdot \log(\frac{d}{d_0}) + X_\sigma \tag{2.3}$$

To illustrate this model, Fig. 6 provides three simulated data sets (blue, red and black). The simulations created data points at 27 different T-R distances for three different values of n. In each case, path-loss increases as the T-R distance becomes large and the path-loss exponent, n, determines the rate of this increase. Higher n (e.g. n = 4,

blue data) leads to quicker decay of the signal, which is represented by larger slope in the figure. At a certain T-R distance, we generated 10 data points. Path-loss varies for each of the 10 data points, which is the result of shadowing component. The range of the variation is dependent on the standard deviation, σ (in dB).

The log-normal shadowing model, to some extent, improves the representation of propagation environment by taking into account the variability of the signal power at some distance. However, this model still has limitations and it is not suitable for all communication environments. For example, when there are lots of obstacles and no line of sight. In this situation, small-scale effects (i.e., multipath) must also be accounted for, for which the Rayleigh fading model is often used [8] [9].

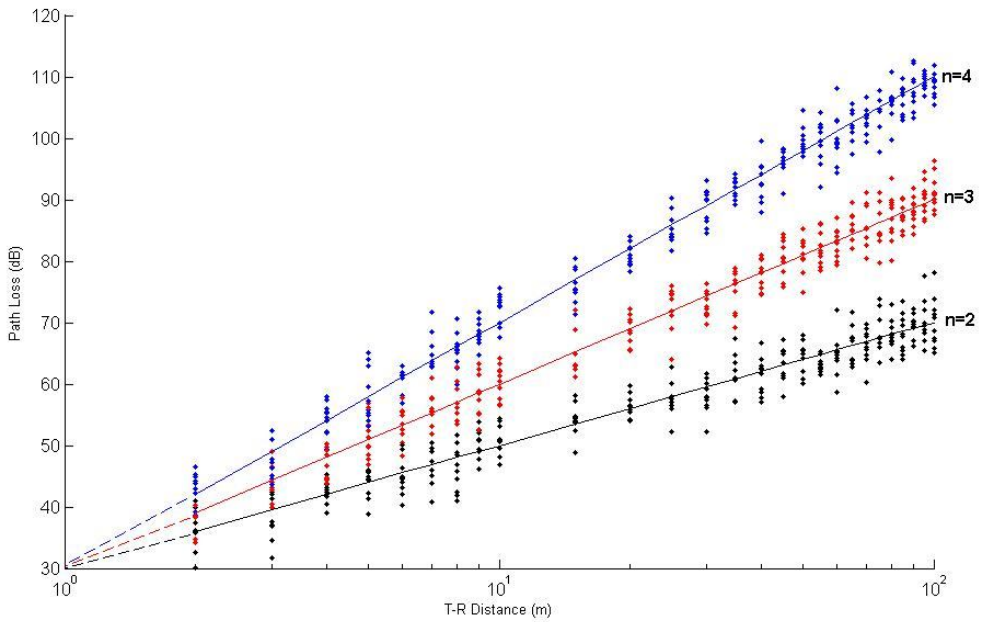

Figure 6. Path-Loss vs. T-R Distance (σ = 3)

2.4 Connecting Footprints with Energy Needs

If one wishes to communicate with farther nodes, the most direct approach is to simply increase the transmission energy. But if this approach is used, how does the added transmission energy impact the node's overall energy availability and lifetime? This question is what the energy models try to answer.

The simply energy model—'Path-Loss Model' can be expressed as follow [12]:

$$E = E_t + E_r = \alpha + \beta \cdot d^n \tag{2.4}$$

Where the energy cost per bit, E, over the distance d includes both the transmitting E_t and receiving E_r energy. α is the energy cost of transmitter and receiver electronics; β is the transmit amplifier constant; n is the pass loss exponent. Equation (2.4) emphasizes that energy costs are proportional to transmission distance (i.e., footprint size). [13][14] added the energy consumed for processing data to the transmission energy, which resulted in the equation:

$$E = E_t + E_r = \alpha + \beta \cdot d^n + E_p \tag{2.5}$$

Where E_p is the data processing energy.

The path-loss model above is simple and easy to calculate, but the model still assumes that the communication contour of the sensor is continuous and isotropic. However, as already discussed, the transmission of the signal is affected by the environment, such as obstacles and geometric conditions. Most propagation environments are not homogeneous and thus n alone can not capture the heterogeneity.

As noted, our work aims to provide better footprint methods which can subsequently be used to better understand the energy needs for sensor nodes.

2.5 Early Usability Results

Because of the shadowing caused by the environment, there will be pockets in a footprint with high signal loss. So if a signal threshold is set, which is the minimal received power needed to have a reliable link, we will want to know the usability of some area. 'Usability' is percentage of the area that will be truly covered, i.e., having signal power higher than the threshold. The usability of circular (unit disc) coverage has been analyzed in the context of cellular systems [8]. In cellular systems, the communication occurs between cellular towers and mobile phones. Cellular transmitting towers are typically 150-270 feet in height [17]. So a line-of-sight can be expected between the top of the tower and a good portion of the coverage area. Thus, the disc model is a good choice for cellular systems. Using nomenclature and results presented in [8], usability, $U(\gamma, R)$, of an area of radius R (i.e. circular disc) is the percentage of the area with received power higher or equal to γ, was calculated by the following equation:

$$U(\gamma, R) = \frac{1}{\pi R^2} \int \Pr[P_r(r) > \gamma] \cdot dA = \frac{1}{\pi R^2} \int_0^{2\pi} \int_0^R \Pr[P_r(r) > \gamma] \cdot r \cdot dr \cdot d\theta \qquad (2.6)$$

In which, $\Pr[P_r(r) > \gamma]$ is the probability $[\Pr]$ that the received power $[P_r]$ at distance r from the transmitter exceeds the connectivity threshold γ.

According to log-normal shadowing model, equation (2.3), $\Pr[P_r(r) > \gamma]$ can be described as:

$$\Pr[P_r(r) > \gamma] = Q\left(\frac{\gamma - \overline{P_r(r)}}{\sigma}\right) = \frac{1}{2} - \frac{1}{2} erf\left(\frac{\gamma - \overline{P_r(r)}}{\sigma\sqrt{2}}\right)$$

$$= \frac{1}{2} - \frac{1}{2} erf\left(\frac{\gamma - \left[P_t - \left(\overline{PL}(d_0) + 10n\log(r/d_0)\right)\right]}{\sigma\sqrt{2}}\right) \qquad (2.7)$$

Where, again, *n* is the path loss exponent and σ is the standard deviation of the Gaussian process (in dB). To solve the above equation, we utilize the *Q function* [8] and the *error function (erf)* [8], which have the following properties:

$$Q(z) = \frac{1}{\sqrt{2\pi}} \int_z^\infty \exp\left(-\frac{x^2}{2}\right) dx = \frac{1}{2}\left[1 - erf\left(\frac{z}{\sqrt{2}}\right)\right]$$

$$Q(z) = 1 - Q(-z)$$

$$erf(z) = \frac{2}{\sqrt{\pi}} \int_0^z e^{-x^2} dx$$

These functions are introduced to analyze the probability of the Gaussian distribution, on which the log-normal shadowing model is based.

Since $\frac{r}{d_0} = \frac{r}{R} \cdot \frac{R}{d_0}$, we have

$$\overline{PL}(r) = 10n\log\left(\frac{r}{d_0}\right) + \overline{PL}(d_0)$$

$$= 10n\log\left(\frac{R}{d_0}\right) + 10n\log\left(\frac{r}{R}\right) + \overline{PL}(d_0) \qquad (2.8)$$

Substituting the expressions in (2.7) with (2.8), $\Pr[P_r(r) > \gamma]$ can be expressed as:

$$\Pr[P_r(r) > \gamma] = \frac{1}{2} - \frac{1}{2} erf\left(\frac{\gamma - \left[P_t - \left(\overline{PL}(d_0) + 10n\log(R/d_0) + 10n\log(r/R)\right)\right]}{\sigma\sqrt{2}}\right)$$

Letting $a = \left(\gamma - P_t + \overline{PL}(d_0) + 10n\log(R/d_0)\right) / \sigma\sqrt{2}$,

and $b = (10n\log e)/\sigma\sqrt{2}$.

The path-loss at the boundary, where $r = R$, becomes

$$\Pr[P_r(R) > \gamma] = \frac{1}{2} - \frac{1}{2}erf(a)$$

Finally, the usability within the boundary is given by

$$U(\gamma, R) = \frac{1}{2} - \frac{1}{R^2}\int_0^R r \cdot erf\left(a + b\ln\frac{r}{R}\right)dr$$

$$U(\gamma, R) = \frac{1}{2}\left(1 - erf(a) + \exp\left(\frac{1-2ab}{b^2}\right)\left[1 - erf\left(\frac{1-ab}{b}\right)\right]\right). \quad (2.9)$$

In Fig. 7, each curve represents a specific value of the boundary coverage; i.e., percentage of boundary locations where the signal exceeds the threshold γ. We determine the usability of the footprint by first calculating equation (2.9) as a function of σ/n (such as presented in [8]). For example, if the path-loss exponent, n, and standard deviation, σ, are both 3, then

$$\frac{\text{Standard Deviation}}{\text{Path - Loss Exponent}} = \frac{3}{3} = 1.$$

In this case our usability result will lie along the line defined by the x-axes being 1. If the probability of signal being higher than the threshold at the boundary is known to be 60%, then the usability of the total area within the boundary will be 89.7%. As seen in Fig. 7, this result is found from following the 60% edge of coverage curve, back to the x-axis value of $\sigma/n = 1$ and then determining the y-axis term (89.7%).

As illustrated in Fig. 7, the usability within a footprint increases in accordance with the boundary probability. For example, if the boundary is closer to the transmitter, higher

boundary connectivity can be expected. Likewise, the usability of footprint should increase. On a specific curve, the usability decreases as the value of σ/n increases. Since higher shadowing component leads to greater chance of pockets with no connectivity, the usability will decrease as σ increases. In addition, if the propagation environment has lower n, the signal power will drop more slowly with distance there. So the slope of the curve decreases as σ/n increases.

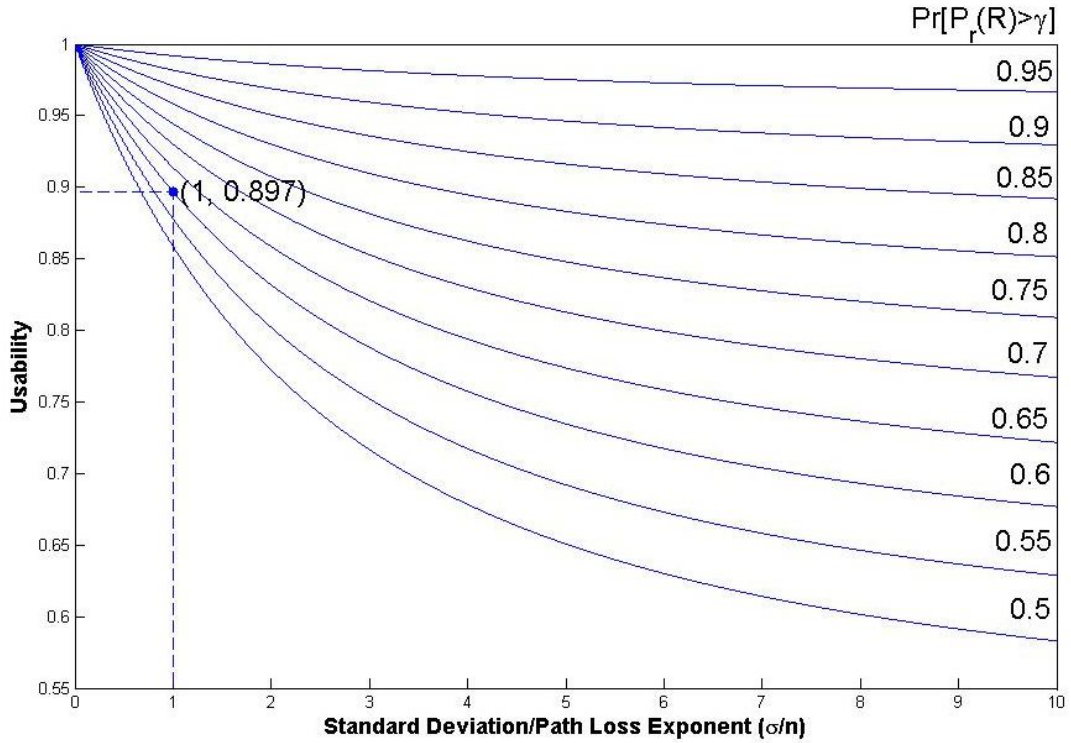

Figure 7. Curves of usability for circular coverage and log-normal shadowing environments

2.6 Conclusion

This chapter introduced the W-M model that provides a method to overcome the main limitation of the disc model which is ignoring the non-isotropic properties of actual footprints. The log-normal shadowing model has been discussed in this chapter as well. This model uses a random variable to characterize the variance of signal power at some distance due to non-homogeneous environments. Based on the log-normal shadowing model, the usability analysis was introduced, which describes the percentage of some area with signal strength higher than some threshold. However, these early usability analyses were built upon the disc model. A usability analysis of the W-M model will be presented in the next chapter.

CHAPTER 3

USABILITY ANALYSIS FOR THE WEAK-MONOTONICITY MODEL

3.1 Introduction

While early usability results based on the disc model were appropriately derived for cellular systems, these results are not suitable for wireless sensor networks. Sensor nodes tend to be embedded on or within structures and thus may not have a line of sight view to adjacent nodes. We contend that the W-M model is a better footprint model, since it allows us to account for heterogeneity. However, in practice footprints are neither purely directional, as given by the W-M model. As such, we propose that by using multiple W-M footprints, one can represent complex footprints. For example, in Fig. 8, three overlapping W-M circles with different radii, *R1, R2, R3,* and angles between successive circles, $\theta 1, \theta 2, \theta 3$, are shown, the contour of which is the footprint of the node. In this chapter, we first analyze the usability of a single W-M circle. Then we use simulations to characterize the usability of footprints with multiple W-M circles such as shown in Fig. 8.

3.2 Derivation of Usability for the W-M Model

In the earlier analysis of the usability (2.5), which is based on the traditional disc model, a node is located at the center of the disc at point *'o'*, and the distance from the node to any other node '*m*' is '*r'*, which is the length of $\overrightarrow{om}$ (Fig. 9). However, in the 'Weak-Monotonicity' model, the node will no longer be at the center but should be on the

boundary of the disc area. Let the point *'p'* be the node as illustrated in Fig. 9, so the distance from it to '*m*', which is *'d'*, will be the length $\overrightarrow{pm}$.

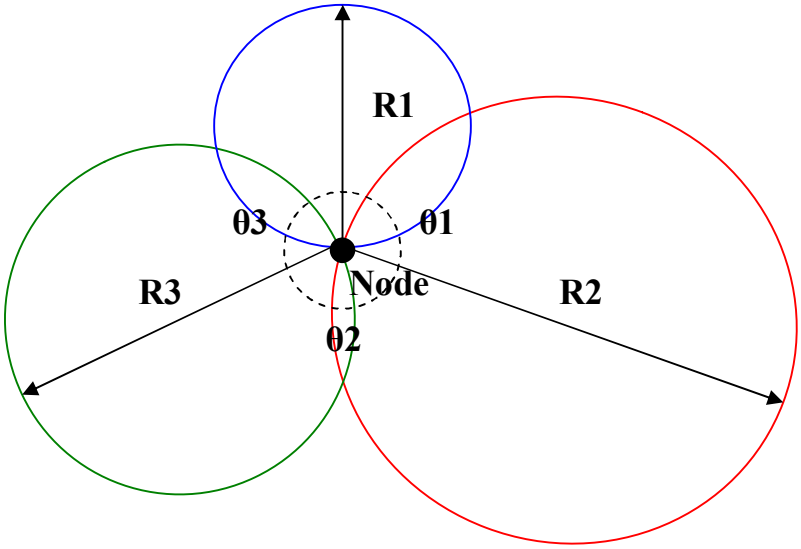

Figure 8. Proposed improved footprint consisting of three overlapping W-M circles

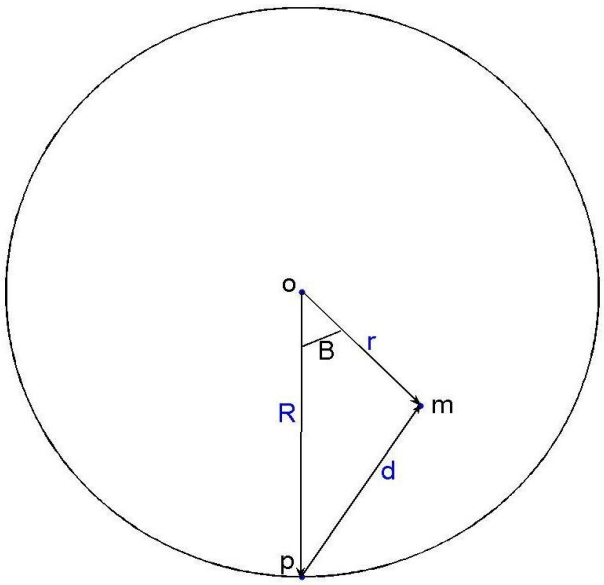

Figure 9. Geometry for usability analysis of the W-M model

By the law of cosines,

$$\left|\overrightarrow{pm}\right|^2 = \left|\overrightarrow{op}\right|^2 + \left|\overrightarrow{om}\right|^2 - 2\left|\overrightarrow{op}\right|\left|\overrightarrow{om}\right|\cos(\angle mop)$$

or $$d^2 = R^2 + r^2 - 2Rr\cos B;$$

giving $$d = \sqrt{R^2 + r^2 - 2Rr\cos B}\ . \qquad (3.1)$$

Thus we find the relation between the T-R distance in the new model, variable '*d*', and the old model, variable '*r*'. We can now use the equations in the early analysis to acquire results for the W-M model.

Recalling equation (2.6) and (2.7), we have

$$U(\gamma, R) = \frac{1}{\pi R^2}\int \Pr[P_r(r) > \gamma]\cdot dA = \frac{1}{\pi R^2}\int_0^{2\pi}\int_0^R \Pr[P_r(r) > \gamma]\cdot r\cdot dr\cdot d\theta$$

Where $$\Pr[P_r(r) > \gamma] = Q\left(\frac{\gamma - \overline{P_r(r)}}{\sigma}\right) = \frac{1}{2} - \frac{1}{2}erf\left(\frac{\gamma - \overline{P_r(r)}}{\sigma\sqrt{2}}\right)$$

$$= \frac{1}{2} - \frac{1}{2}erf\left(\frac{\gamma - \left[P_t - \left(\overline{PL}(d_0) + 10n\log(r/d_0)\right)\right]}{\sigma\sqrt{2}}\right) \qquad (3.2)$$

Resulting in

$$U(\gamma, R) = \frac{1}{\pi R^2}\int_0^{2\pi}\int_0^{\mathrm{R}}\left\{\frac{1}{2} - \frac{1}{2}erf\left(\frac{\gamma - \left[P_t - \left(\overline{PL}(d_0) + 10n\log(d/d_0)\right)\right]}{\sigma\sqrt{2}}\right)\right\}\cdot r\cdot dr\cdot d\theta \qquad (3.3)$$

For the W-M analysis, we note that angle $\theta = B$ in Fig. 9 and that we need to replace the *r*, which is distance in the old model, with the new *d*.

Given equation (3.1), equation (3.3) becomes

$$U(\gamma,R)=\frac{1}{\pi R^2}\int_0^{2\pi}\int_0^{\mathrm{R}}\left\{\frac{1}{2}-\frac{1}{2}erf\left(\frac{\gamma-\left[P_t-\left(\overline{PL}(d_0)+10n\log\left(\sqrt{R^2+r^2-2Rr\cos\theta}\cdot\frac{1}{d_0}\right)\right)\right]}{\sigma\sqrt{2}}\right)\right\}\cdot r\cdot dr\cdot d\theta$$

We rewrite the above into two integrals.

$$U(\gamma,R)=\frac{1}{\pi R^2}\int_0^{2\pi}\int_0^{\mathrm{R}}\frac{1}{2}\cdot r\cdot dr\cdot d\theta$$
$$-\frac{1}{2\pi R^2}\int_0^{2\pi}\int_0^{\mathrm{R}}erf\left(\frac{\gamma-\left[P_t-\left(\overline{PL}(d_0)+10n\log\left(\sqrt{R^2+r^2-2Rr\cos\theta}\cdot\frac{1}{d_0}\right)\right)\right]}{\sigma\sqrt{2}}\right)\cdot r\cdot dr\cdot d\theta \tag{3.4}$$

The first integral on the right side of equation (3.4) can be calculated out as follows:

$$\frac{1}{\pi R^2}\int_0^{2\pi}\int_0^{R}\frac{1}{2}\cdot r\cdot dr\cdot d\theta=\frac{1}{\pi R^2}\int_0^{R}\left(\frac{1}{2}\cdot r\cdot\int_0^{2\pi}d\theta\right)\cdot dr$$
$$=\frac{1}{\pi R^2}\int_0^{R}\pi\cdot r\cdot dr=\frac{1}{\pi R^2}\cdot\left(\frac{1}{2}\pi R^2\right)=\frac{1}{2}$$

To solve the second integral of (3.4) we note that

$$\log\left(\frac{\sqrt{R^2+r^2-2Rr\cos\theta}}{d_0}\right)=\log\left(\frac{2R}{d_0}\cdot\frac{\sqrt{R^2+r^2-2Rr\cos\theta}}{2R}\right).$$

Thus the expression $\overline{PL}(d_0)+10n\log\left(\frac{\sqrt{R^2+r^2-2Rr\cos\theta}}{d_0}\right)$ in (3.4), which represents

the mean path-loss at distance *r*, becomes

$$\begin{aligned}\overline{PL}(r) &= 10n\log\left(\frac{\sqrt{R^2+r^2-2Rr\cos\theta}}{d_0}\right)+\overline{PL}(d_0)\\ &= 10n\log\left(\frac{2R}{d_0}\right)+10n\log\left(\frac{\sqrt{R^2+r^2-2Rr\cos\theta}}{2R}\right)+\overline{PL}(d_0)\end{aligned} \tag{3.5}$$

Replace the expression of mean path-loss in (3.2) with (3.5), $\Pr[(P_r(r)>\gamma)]$ can be expressed as

$$\begin{aligned}&\Pr[P_r(r)>\gamma]\\ &=\frac{1}{2}-\frac{1}{2}erf\left(\frac{\gamma-\left[P_t-\left(\overline{PL}(d_0)+10n\log\left(\frac{2R}{d_0}\right)+10n\log\left(\frac{\sqrt{R^2+r^2-2Rr\cos\theta}}{2R}\right)\right)\right]}{\sigma\sqrt{2}}\right)\\ &=\frac{1}{2}\\ &-\frac{1}{2}erf\left(\frac{\gamma-P_t+\overline{PL}(d_0)+10n\log\left(\frac{2R}{d_0}\right)+10n\log\left(\sqrt{R^2+r^2-2Rr\cos\theta}\right)-10n\log(2R)}{\sigma\sqrt{2}}\right)\end{aligned} \tag{3.6}$$

Bringing (3.6) into (3.4), the usability of the W-M footprint is given by

$$U(\gamma,R)=\frac{1}{2}-\frac{1}{2\pi R^2}\int_0^{2\pi}\int_0^R erf\left[a+b\log\left(\sqrt{R^2+r^2-2Rr\cos\theta}\right)-c\right]\cdot r\cdot dr\cdot d\theta \tag{3.7}$$

where $$a=\frac{\gamma-P_t+\overline{PL}(d_0)+10n\log(2R/d_0)}{\sigma\sqrt{2}},$$

$$b=\frac{10n}{\sigma\sqrt{2}},$$

$$c = \frac{10n}{\sigma\sqrt{2}} \cdot \log(2R).$$

As with the unit circle usability result, we can glean the W-M footprint usability from its coverage at the boundary. For the W-M model, we define the extent of the boundary to be the point of the furthest communication, that is, where $r = 2R$. At the boundary, thus, the coverage percentage is given by

$$\begin{aligned} \Pr[P_r(2R) > \gamma] &= \frac{1}{2} - \frac{1}{2} erf\left(\frac{\gamma - P_t + \overline{PL}(d_0) + 10n\log(2R/d_0)}{\sigma\sqrt{2}} \right) \\ &= \frac{1}{2} - \frac{1}{2} erf(a) \end{aligned} \tag{3.8}$$

No closed form solution to (3.7) is known, and as such we solve it numerically (in our case, using Matlab). For example, given

1) the distance to the farthest node
2) signal threshold
3) power received at reference distance ($d_0 = 1\,m$)
4) path-loss exponent
5) standard deviation for shadowing component

we can calculate the usability by (3.7). To illustrate this method and considering realistic numbers for sensor networks, we have $R = 7.339\,m$; $\gamma = -100\,dBm$; $P_r(d_0) = P_t - \overline{PL}(d_0) = -65\,dBm$; $n = 3$; $\sigma = 3$. Solving (3.7) we find

$$U(\gamma, R) = 92.28\%$$

is the usability for this W-M footprint.

3.3 Analysis of Usability Results

As expected, usability decreases as coverage radius becomes larger. In Fig. 10, $R2 > R1$. Let $C(R1)$ and $C(R2)$ specifically be the coverage area of the footprint with radius *R1* and *R2*. We note that $C(R1) \subset C(R2)$ and the shaded region represents $C(R2) \setminus C(R1)$, which means the area include in $C(R2)$, but not in $C(R1)$. Since the shaded region is further from the transmitter than $C(R1)$, the power received in this shaded area is lower than that of $C(R1)$. Considering that the usability of $C(R2)$ is averaged over $C(R1)$ and the shaded region, the result will be lower than the usability of $C(R1)$.

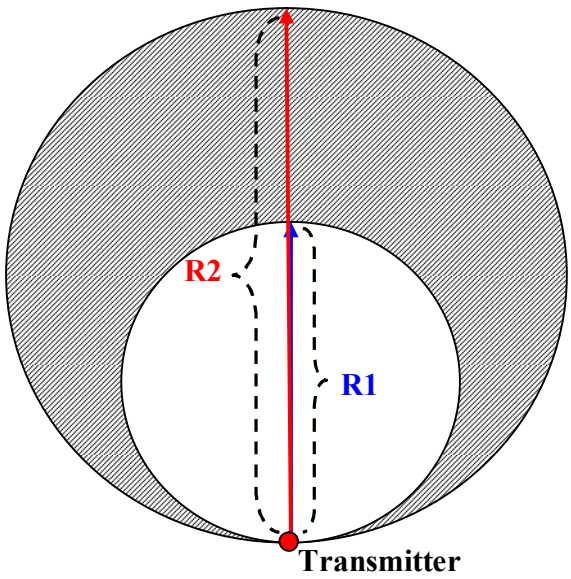

Figure 10. Enlarge of coverage area as increase of radius

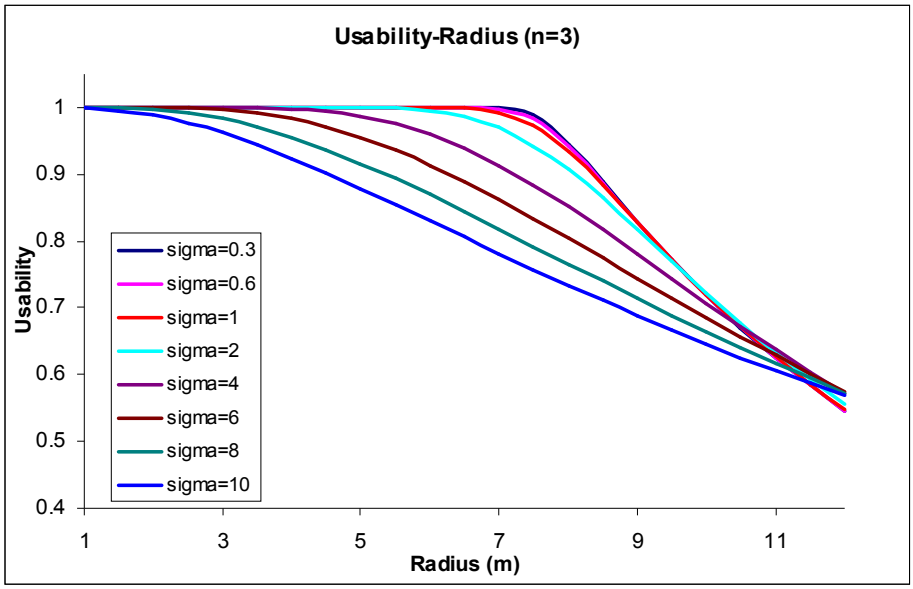

Figure 11. Usability-Radius curves of different shadowing coefficients for fixed path loss exponent (n = 3).

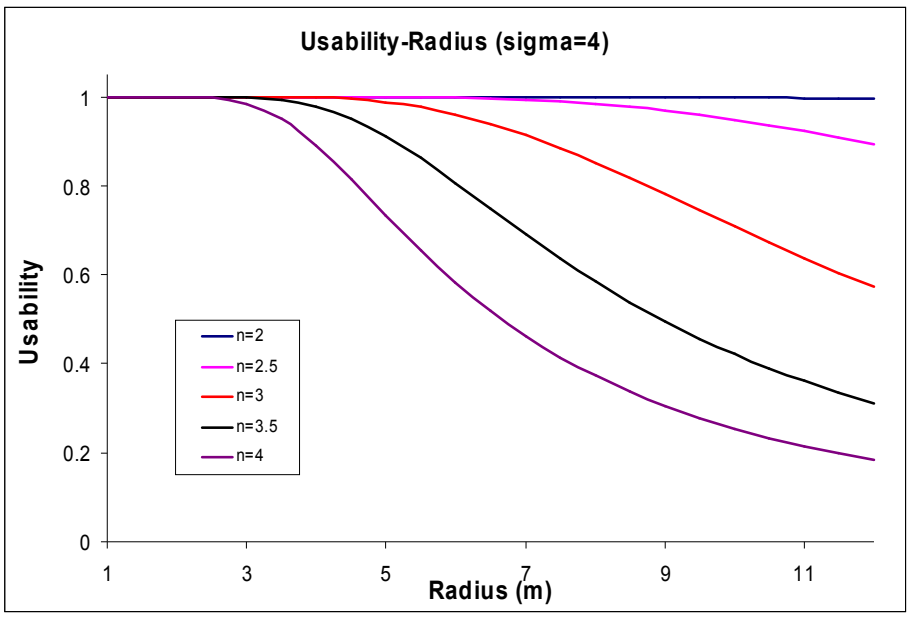

Figure 12. Usability-curves of different path-loss exponent for fixed shadowing coefficient (σ = 4).

Employing our result of (3.7), Figs. 11 and 12 show the curves of usability-radius for various path-loss exponents or shadowing coefficients when fixing the other. Both these figures show that the usability of each curve becomes lower as radius increases. In Fig. 11, n is fixed. Curves representing higher shadowing coefficients have lower usability, which means that greater shadowing effects increase the probability that a signal is lower than the threshold within the footprint. If we look further, we can find out that when the radii are larger than some value, here it is around 11 m, relationship of the curves start inverting. Curves with higher σ become the ones having lower usability, which is as we expected. Since in the further area, the average link reliability is really low, larger σ can offer higher probability of good link (i.e. greater chance of positive interference). In Fig. 12, we can find out that larger n leads to quicker drop of usability as shadowing coefficient fixed.

The usability of W-M footprint is lower than that of a disk footprint having the equivalent maximum T-R distance. This difference between this new result and the earlier analysis of usability is due to that the percentage of the signal above the threshold on the boundary is no longer uniform, since the points on the boundary have various distances from the node, while in the early work they are on the circle centered by the node. However, the influence of n and σ to signal power are the same, following log-normal shadowing model, so we can see same influence on usability in the W-M model and the disc model.

3.4 Simulation for Single Footprint

We expect the analysis of usability with over-lapping weak-monotonicity discs (Fig. 8) to be difficult and thus we will use simulation to analyze such complex footprints. The routines to be discussed are included in the attached CD. To validate the simulation method we first compare its results to the analytical results for a single W-M footprint (Equ. 3.7).

As seen in Fig. 13, we generated nodes, N_i, ($i = 1,2,...$), uniformly deployed on an $L_x(m) \times L_y(m)$ area. We let node *t*, with coordinate $(R, 0)$, be the transmitter and *F*, with coordinate $(R, 2R)$ be the farthest node. R is the radius of the footprint circle. For illustration, in Fig. 13, we have $L_x = L_y = 2R = 16\,m$; $R = 8\,m$.

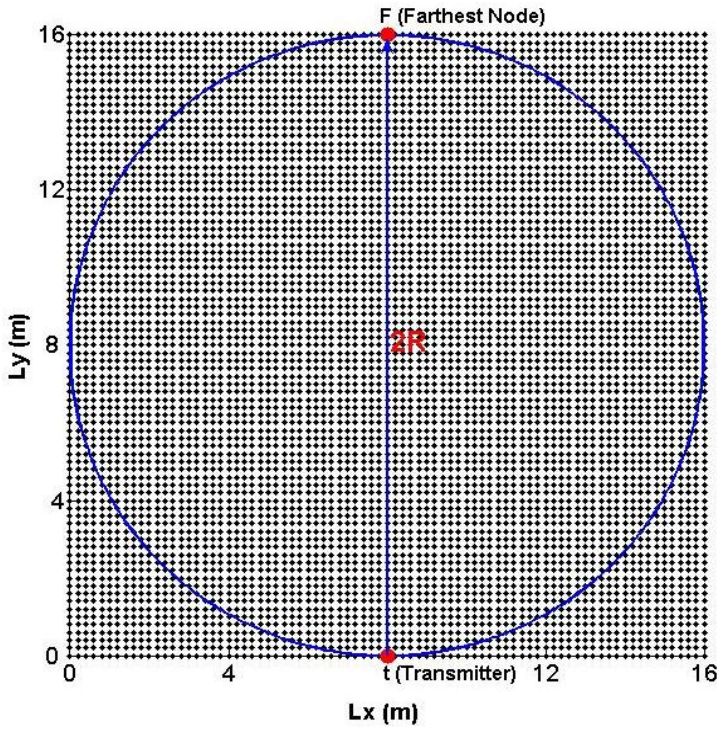

Figure 13. Simulation of 'Weak-Monotonicity' Model with Matlab

Next, we generate Gaussian distributed numbers with zero mean and standard deviation, σ, and let these numbers be the shadowing component, X_σ, of the received signal at each node. Using equation (2.3), the log-normal shadowing model simulates the received power at each node. We consider a reference distance, d_0, of $1\,m$ and $P_r(d_0)$, the power at reference distance, to be $-65\,dBm$. This value $-65\,dBm$ was collected by practical test at distance $1\,m$ when the transmit power is $0\,dBm$. Node F with coordinator $(R, 2R)$ is the farthest node from the transmitter and thus has signal power $P_r(F) = -65\,dBm - 10 \cdot n \cdot \log(2R) + X_\sigma$.

Matlab simulation was then used to find the percentage of nodes with received power higher or equal to the threshold within the footprint area, which is the usability. Fig. 14 illustrates these simulation results, based on the setting of path-loss exponent $n = 3$ and standard deviation $\sigma = 3$. The signal threshold was set at $-90\,dBm$, which is represented in the figure as the horizontal line. $-90\,dBm$ represents a reasonable receiver threshold for low power wireless sensor nodes [12].

This simulated deployment of 6561 nodes uniformly spaced over an area of $16\,m \times 16\,m$ is represented as data points in the figure. The black curve is the average signal power over distance, which is $\overline{P_r}(d) = -65\,dBm - 30\log(d)$. Because of the Gaussian shadowing component, almost all the simulated data points were around the average value within the range of $\pm 2\sigma$, which are represented as red dashed curves. Using this curve, we can calculate the usability of different range as a function of T-R radius as the ratio of the number of points above $-90\,dBm$ to all points (i.e. 6561).

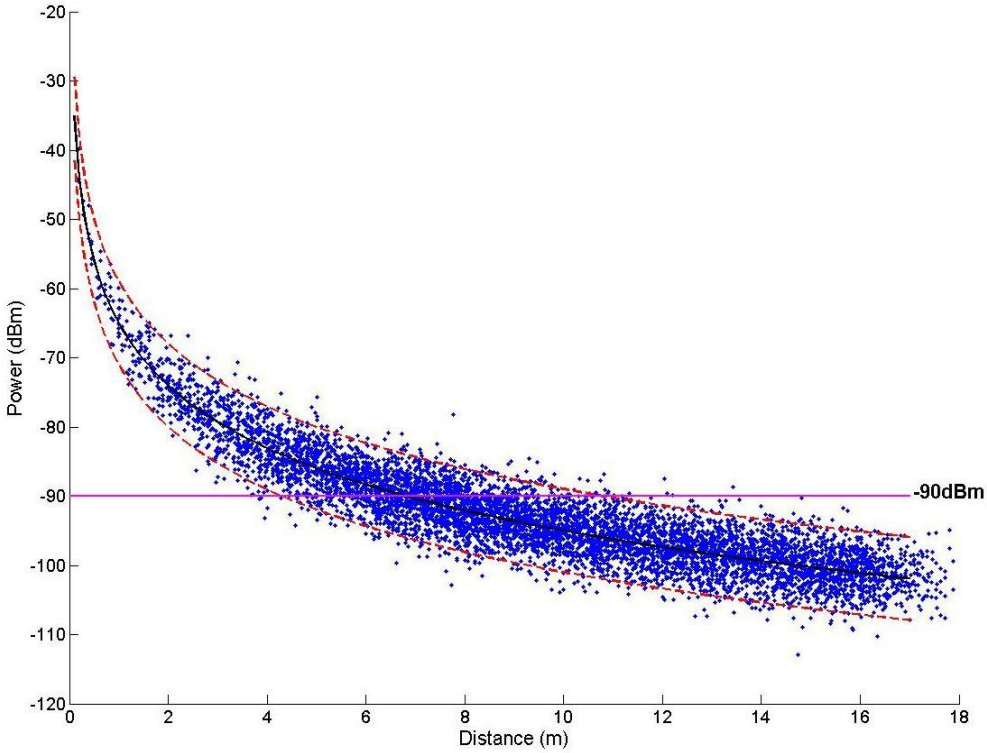

Figure 14. Distance-Power Received curve of simulation ($\sigma = 3$; $n = 3$; 6561 nodes)

Table 1 gives the values of $\hat{U}(r,R)$, average simulated usability, each of which was averaged over 10 simulations. $U(r,R)$ is the value of the theoretical usability calculated using equation (3.5) and R is the radius of the footprint. Both the path loss exponent (n) and shadowing coefficient (σ) are fixed at 3 for these results. Fig. 15 shows the curves of the values in Table 1, from which we can find that the simulation results agree with the theoretical result. The errors between them are quite small, the average of which is 0.22%. Thus our simulation appears to be a good method to analyze usable area within the weakly-monotonic defined footprints.

Table 1. (a) Simulation results (Thresho1d = -90 dBm; $\sigma = 3$; $n = 3$)

Usability (Threshold = -90 dBm; $\sigma = 3$; $n = 3$)											
R	**1m**	**1.5m**	**2m**	**2.5m**	**3m**	**3.5m**	**4m**	**4.5m**	**5m**	**5.5m**	**6m**
$U(r,R)$	1	1	0.999	0.993	0.966	0.910	0.831	0.742	0.655	0.576	0.507
$\hat{U}(r,R)$	1	1	0.998	0.993	0.965	0.910	0.831	0.741	0.659	0.578	0.505

Table 1. (b) Simulation results (Threshold = -90 dBm; $\sigma = 3$; $n = 3$)

Usability (Threshold = -90 dBm; $\sigma = 3$; $n = 3$)										
R	**6.5m**	**7m**	**7.5m**	**8m**	**8.5m**	**9m**	**9.5m**	**10m**	**10.5m**	**11m**
$U(r,R)$	0.448	0.397	0.354	0.317	0.286	0.259	0.235	0.215	0.197	0.181
$\hat{U}(r,R)$	0.450	0.398	0.355	0.318	0.285	0.259	0.234	0.214	0.196	0.181

Table 1. (c) Simulation results (Threshold = -90 dBm; $\sigma = 3$; $n = 3$)

Usability (Threshold = -90 dBm; $\sigma = 3$; $n = 3$)								
R	**11.5m**	**12m**	**12.5m**	**13m**	**13.5m**	**14m**	**14.5m**	**15m**
$U(r,R)$	0.167	0.154	0.143	0.133	0.124	0.116	0.109	0.102
$\hat{U}(r,R)$	0.166	0.154	0.142	0.133	0.124	0.116	0.108	0.102

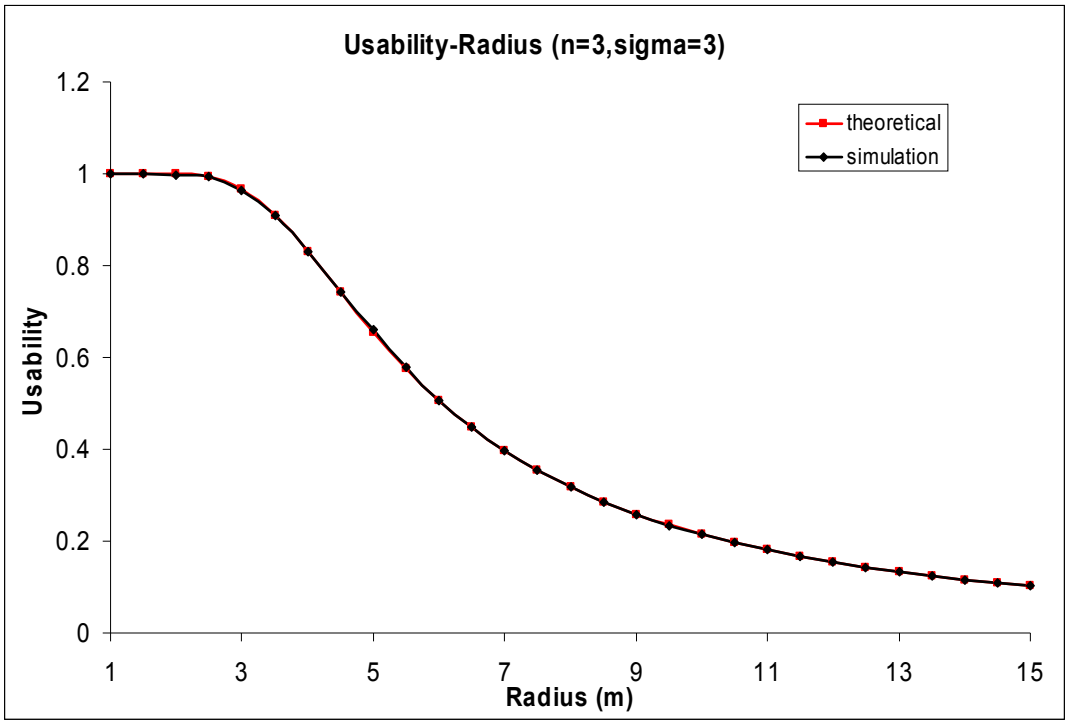

Figure 15. Usability-Radius curve with $n = 3$ and $\sigma = 3$ (From Table 1)

3.5 Simulation of Overlapping W-M Footprints

The above analysis only considers the footprint for a single sensor and one that has directivity. However, in practice, a sensor network may consist of 10s to 100s or more nodes. Sensors will be expected to communicate with other sensors that surround them and thus multiple W-M footprints may be needed to model this. So the situation will be much more complicated than simply adding together the results of multiple W-M footprints. We use our validated simulation method to analyze this new footprint.

As an example, Fig. 16 gives an example footprint created using three overlapping W-M footprints with equal radii, separated by 120°. The usability results of this example

are illustrated in Fig. 17 together with the simulation results of the disc model with single footprint circle of radius *R*. We note from this result that the usability of W-M model is higher than the disc model for a given T-R distance. This should not be surprising since the W-M based footprint's coverage is weighted closer to the center of coverage. However, what is significant is that the usability predicted by the disk model is too conservative if indeed isotropic connectivity is not the case. The over-conservative model would lead to over-deployment of sensors to achieve the desired link reliability. That being said, by incorporating shadowing in our footprint, our W-M model will be more conservative than that presented in [3] where within the footprint connectivity was assumed to be guaranteed.

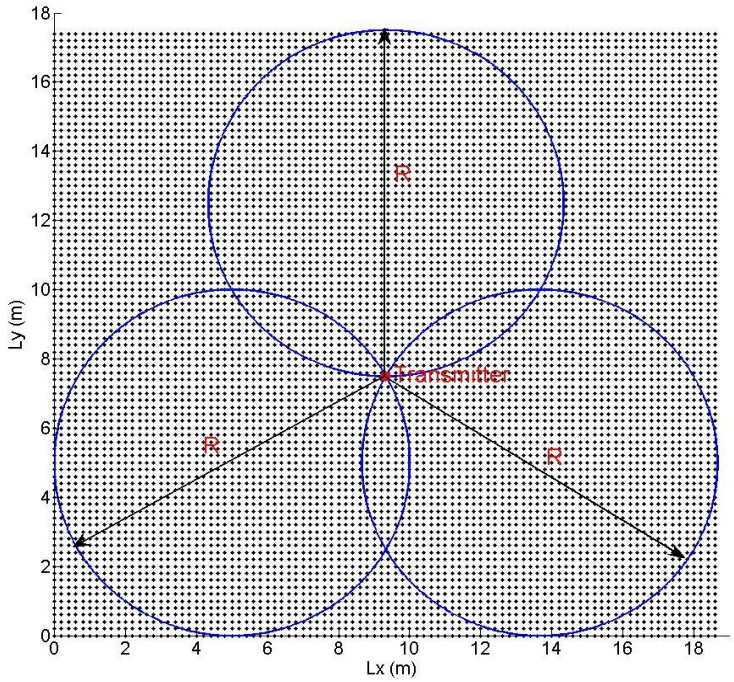

Figure 16. Three equal radii overlapping W-M model example

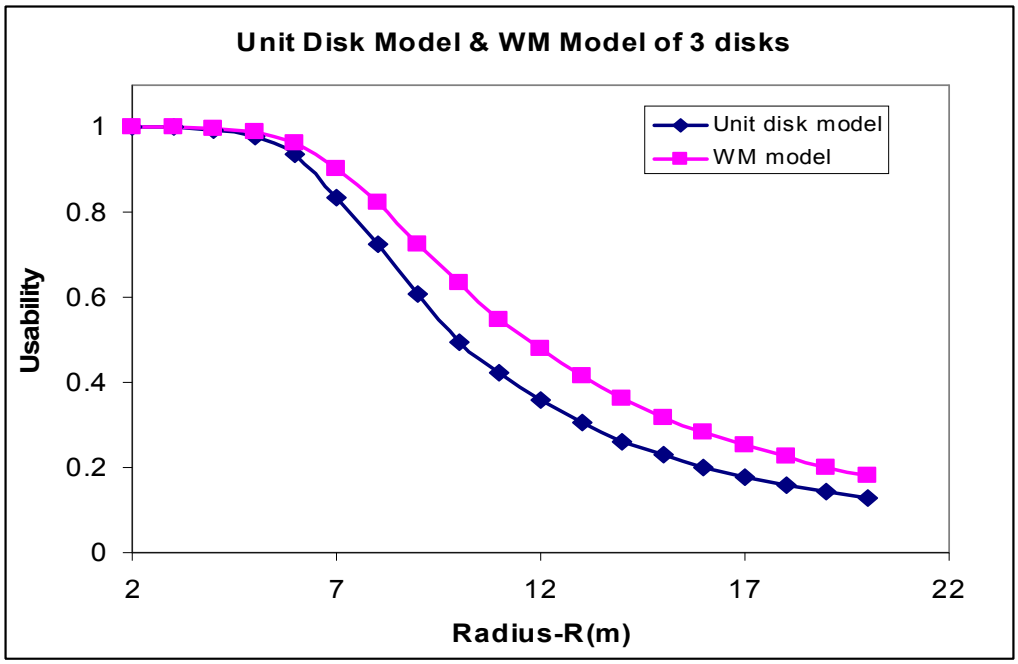

Figure 17. Usability vs. radius curve for W-M based footprint and a unit disk

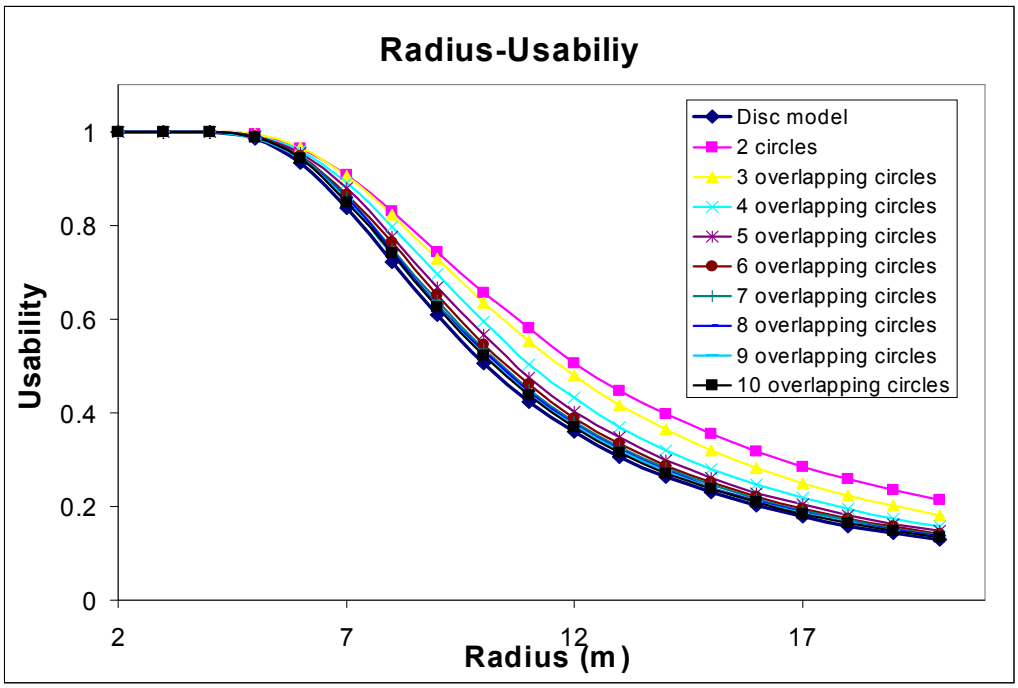

Figure 18. Usability vs. radius curve for multiple overlapping footprint circles

Fig. 18 shows the usability curves of multiple overlapping circles. As the number of circles increases (Fig. 19), the usability gets closer to the disc model. This result is easy to understand, because with the increase of circles, the whole footprint becomes more like the disc model. This result gives us another point of validation of our simulation.

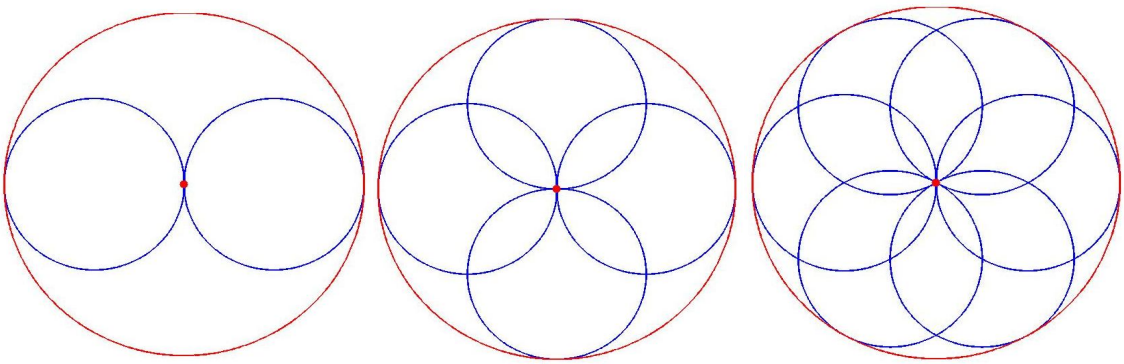

Figure 19. Different number of overlapping footprint circles compared with disc model

Obviously the scenarios presented are purely illustrative, but since real environments may have many obstacles, signal propagation will highly depend on the direction and range. As such, we can use our W-M approach to create a general footprint model (such as illustrated in Fig. 8) for an individual node having an arbitrary number of lobes, with arbitrary radii and angles as given by (3.9).

$$footprint = \bigcup_{i=1}^{N} WM(R_i, \theta_i) \tag{3.9}$$

With (3.9), simulations of networks can now be developed in which the footprint parameters for each node (N, R, θ) can be uniquely defined or provided randomly through distributions.

3.6 Conclusion

The derivations of the usability for W-M model were presented in this chapter. This result was used to validate an alternative analysis approach using simulation. The results of these two methods have been shown to agree quite well. The simulation work has been further validated in the scenarios with overlapping W-M circles. In the next chapter, these overlapping scenarios of W-M model will be used to develop footprints to represent empirical data.

CHAPTER 4

DEVELOPING A W-M BASED MODEL FOR EMPIRICAL DATA

4.1 Introduction

In this chapter, we leverage the overlapping W-M model to develop footprints for empirical data collected in three indoor settings. First, the locations, equipment and test set up for the measurements are introduced. We then analyze the empirical data collected to ascertain the log-normal shadowing parameters. Finally, a W-M based footprint is proposed to matche each scenario.

4.2 Test Method

To illustrate the use of our proposed W-M based footprint, we collected path loss data for three indoor scenarios. The data was collected in the corridors on the 3rd floor of Votey Hall at the University of Vermont:

The following equipment was used:

– A-Systems Inc. signal generator (Fig. 20a)

– Rohde & Schwarz FSH6 spectrum analyzer (100 KHz-6 GHz) (Fig. 20b)

– Tape measures are used to determine the T-R distance in our measurements.

(a) Transmitter: A System Inc signal generator

(b) Receiving spectrum analyzer: Rohde & Schwarz FSH6 spectrum analyzer

Figure 20. Main equipment

The set up is shown in Fig. 21. The transmitter height was set to 72 *cm* (Fig. 22). The receiving antenna was fixed at the height of 70 *cm* and connected to the spectrum analyzer (Fig. 23). The frequency was set to 2.4 GHz, the lower end of the frequency band commonly used for sensor networks, and the transmitting power to $0\,dBm$. Data was collected every $0.5\,m$, from 1 *m* to 10 *m* (T-R distance) in each direction. Since the width of the corridor is 2.6 *m*, in some directions we could not reach 10 *m*.

Figure 21. Measurement set up

Figure 22. Transmitter height is 72 *cm*

Figure 23. Receiving antenna and spectrum analyzer

4.3 Scenario I

4.3.1 Application

For Scenario I, the signal transmitter is put by one side of the corridor at 3rd floor in Votey Hall. This scenario may represent a wall mounted network that communicates down a long corridor. We took measurements every 0.5*m* from 1*m* to 10*m*, in 19 different directions, from 0° to 180°, as in Fig 24. In Fig. 24, data was collected at each intersection of the radial and circular lines. 222 data points in total were collected for this scenario. When a sensor node is deployed in a narrow place and located really close to a

large obstacle on one side, like this scenario, the footprint constructed by this scenario can be applied, since the footprint will be really similar.

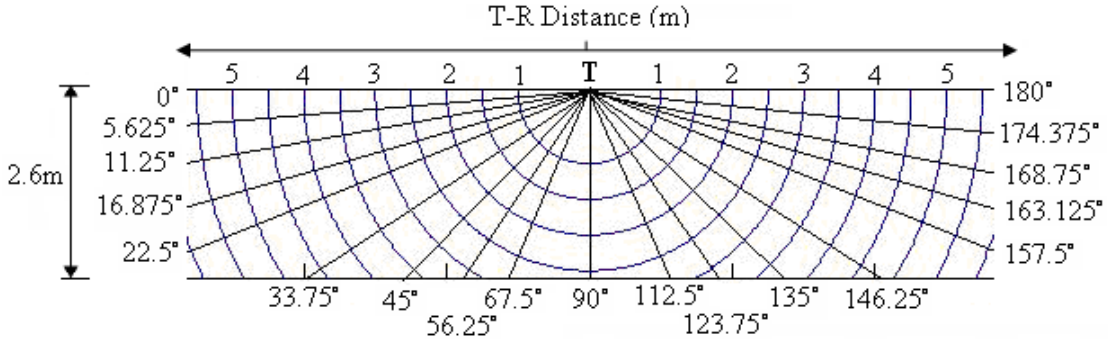

Figure 24. Measurement locations for Scenario I

4.3.2 Data

Table 2. (a) Data set for Scenario I

Scenario I: Measurement Data (-dBm)										
		Angle (Degree)								
		0	**5.625**	**11.25**	**16.875**	**22.5**	**33.75**	**45**	**56.25**	**67.5**
T-R Distance (m)	**1**	40.1	40	36.4	38.5	37.3	39.3	41.2	40.3	41.5
	1.5	45.7	40.6	41.6	39.6	42.1	39.3	40.3	38	40.1
	2	46.8	39.9	45.2	43.5	44.7	42.9	42.6	40.2	42
	2.5	48.5	43.7	43.9	44.4	42.6	48	43	44.2	45.5
	3	50.5	48.1	45.8	48	43.3	45.1	47.9	41.3	
	3.5	50.4	49.4	47	48.1	46	47.3	48.3		
	4	55.2	47.4	49.6	48.3	49.6	50.8			
	4.5	49.2	47.6	49.1	47	48	49.6			
	5	55.3	48.1	47.5	48	50.6				
	5.5	59	49.2	50.8	53.9	50.4				
	6	63.7	54.3	52	53.1	49.6				
	6.5	68.5	48.5	49	55	50				
	7	55.7	50.2	49.6	51					
	7.5	54.6	49.7	51.3	51.6					
	8	60.8	52.3	52.4	58.4					
	8.5	56.5	52.8	53.6	56.9					
	9	69.9	60.4	58.9	63					
	9.5	66	55.5	56.3						
	10	56.4	60.5	56						

Table 2. (b) Data set for Scenario I

Scenario I: Measurement Data (-dBm)											
		Angle (Degree)									
		90	**112.5**	**123.75**	**135**	**146.25**	**157.5**	**163.125**	**168.75**	**174.375**	**180**
T-R Distance (m)	**1**	40.2	40.5	38.3	40.7	41	42.9	41.1	44	38.6	40.3
	1.5	39.7	42.4	40.5	40.7	41.3	39.7	40.5	45.2	42.2	42.2
	2	43.5	41.8	41.3	42.1	43.7	41.9	42.3	47.5	41.4	41.5
	2.5	44.6	43.6	41.8	47.2	48.5	46.4	45.1	42.7	44.2	46.4
	3			43	44.2	48.8	42.3	47.2	43.3	43.8	53.8
	3.5				52.9	48	44.9	53.9	45.1	48.2	46
	4					48.7	46.8	47.7	46.9	57.2	55.7
	4.5					46.4	48.6	51.8	44.2	45.3	53
	5						48.5	51.7	49.3	55.4	61.8
	5.5						50.1	54.8	46.6	49.4	61.2
	6						50.9	53.8	51.7	51.5	58.6
	6.5						47.9	52.8	52.7	50.2	56.5
	7							55.8	50.8	50.8	55.3
	7.5							57.6	50.5	50.2	67.7
	8							51.5	50.4	57	63.2
	8.5							68.9	53	55.3	65.4
	9							57.3	56.5	59.3	68.1
	9.5								57	58.5	62.9
	10								58.5	57.1	70.6

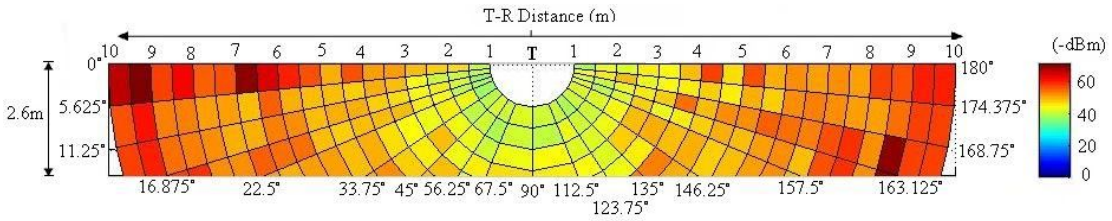

Figure 25. Color map for Scenario I

The empirical data we collected in Scenario I is listed in Table 2. In order to give a better description of the signal power in this scenario, Fig. 25 shows the color map of the data, in which we use colors to represent different signal power. The standard deviation of all data in our measurements is about 0.44 *dB*, which is obtained by taking 10 data points at a specific location and calculating the standard deviation of these 10 data.

4.3.3 Analysis

The raw data from our measurements is provided in Table 2. In the following discussion, we will characterize the measurements using the parameters found in the log-normal shadowing model (i.e. n and σ). This approach is often taken using the entire data sets [8]. We will also do such global characterizations. However, to assist in our development of the overlapping W-M footprint, we will ascertain these parameters as a function of measurement direction as well.

Fig. 26 illustrates the data points of Table 2 and path-loss exponents. Each line represents a linear relationship between the signal power and $10 \times \log(\frac{d}{d_0})$, so the slope of it is the path-loss exponent, n, in this direction. As expected, we find out from Fig. 26 that all lines have positive slopes, which means in all direction signal power drops as the T-R distance gets bigger. Most of the data points do not exactly fall on the linear lines. They scatter around the lines, which can be explained by the existence of the shadowing. The average of all n shown in the figure is 2.06. We only average over the directions in which the T-R distance can reach $9m$, ignoring directions having fewer data. In those longer directions, shadowing coefficients are also calculated and listed in Table 3, the average of which is 2.6. Fig. 27 plots the curves of n and σ at different directions. We find that the curves both have symmetry in that higher at two ends and lower in the middle. This is as what we expected, because the environments are symmetric about 90°. As shown in Fig. 24, the two ends of curves represent the directions close to the wall (i.e. closer to 0° and 180°), while the middle ones represent the directions in between, further

to the wall. The *x*-axis represents the direction number, which we define in the row of 'Direction' in Table 3.

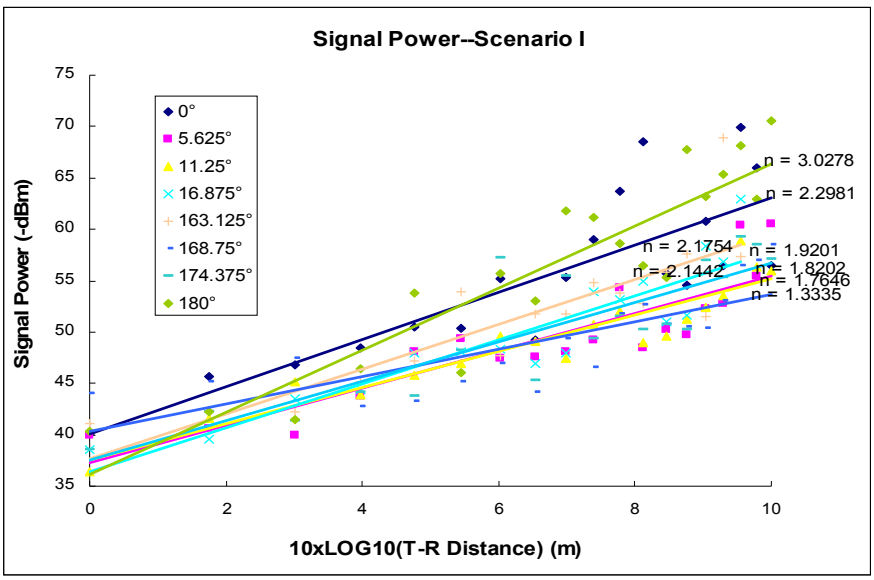

Figure 26. Signal power vs. T-R distance (Scenario I)

Table 3. Shadowing coefficient (σ) and path loss exponent (n) for Scenario I

Angle (°)	0	5.625	11.25	16.875	163.125	168.75	174.375	180	Aver-
Direction	1	2	3	4	5	6	7	8	age
n	2.298	1.820	1.765	2.144	2.175	1.333	1.920	3.028	2.0605
σ	4.402	2.591	1.763	2.366	3.478	2.744	3.100	3.463	2.6009

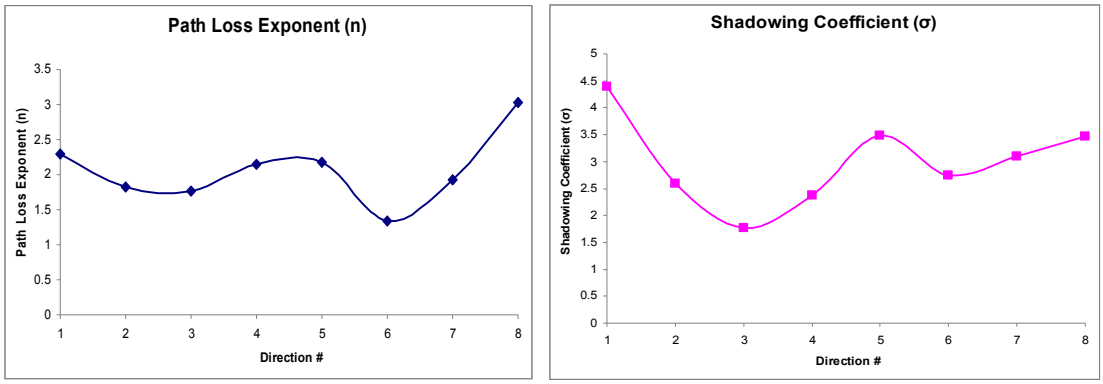

Figure 27. *n* and *σ* distribution for Scenario I

4.3.4 Proposed Method for Determining W-M Footprint

If we assume that receiving signal powers at the reference distance, d_0, are P_0, same in all directions and ignore shadowing coefficients, signal power at T-R distance d will be

$$P(d) = P_0 - 10n\log(\frac{d}{d_0}). \tag{4.1}$$

By (4.1), we can find out that for specific receiving power level P, the T-R distance is

$$\log\left(\frac{d}{d_0}\right) = \frac{P_0 - P}{10n}. \tag{4.2}$$

In different directions

$$\frac{\log\left(\frac{d_1}{d_0}\right)}{\log\left(\frac{d_2}{d_0}\right)} = \frac{n_2}{n_1}. \tag{4.3}$$

Let $d_0 = 1$, then

$$\frac{\log d_1}{\log d_2} = \frac{n_2}{n_1}. \tag{4.4}$$

So the relationships between the radii of W-M circles in directions with different path-loss exponents are built. For example, if we know that in direction *i*, path-loss exponent, n_i, equals 2 and in another direction *j*, $n_j = 3$, we can get $\frac{n_i}{n_j} = \frac{2}{3}$. So if we set a signal power threshold as the boundary of the W-M circle, the radii of the W-M circles in these two directions will have the relationship $\frac{\log r_i}{\log r_j} = \frac{3}{2}$, where r_i and r_j specifically represent the radius of direction *i* and *j*. Since we have calculated out path-loss coefficients in different directions, we propose to build a W-M circle in each of these direction and the relationships between the radii of these circles are derived from equation (4.4).

From equation (4.4), we can find that the relationship is logarithmic. So, small differences in *n* will lead to large differences in radii. Considering this problem, we plot the W-M footprint for Scenario I in logarithm scale in Fig. 28. So the ratio of radii for any two circles equals to the ratio of *n* for these two directions. Thus the differences of radii are not too large now and can be kept in one figure. We can get a better idea of what the footprint look like from Fig. 28. The radii of circles are based on the value of *n* in Table 3. In directions with lower *n*, the circles are larger than other directions. These circles are overlapping with each other. The contour of them is regarded as the footprint of the transmitter, 'T'. If we change the signal threshold P_0, the radii of all circles will change, but the relationship between them does not change. So the shape and the contour of the footprint will be same.

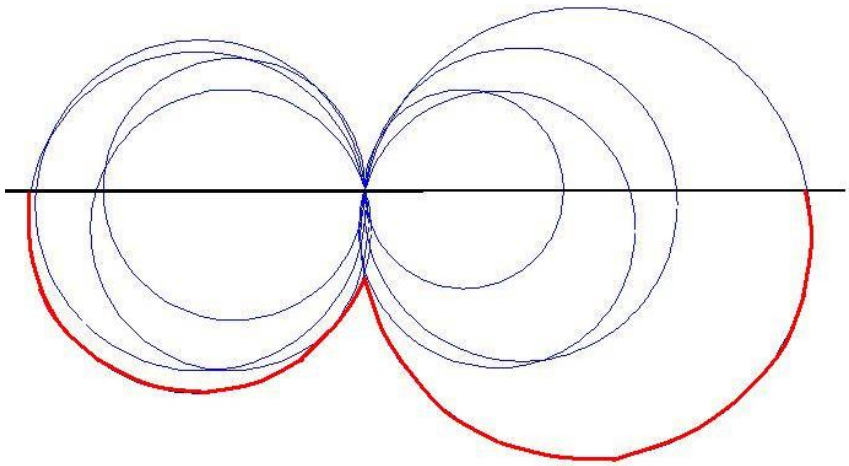

Figure 28. W-M footprint for Scenario I in logarithmic scale

Even though the W-M footprint in Fig. 28, marked by red curve, does not fit perfectly with data in Table 2 and Fig. 25, it is better than the disc model, which would make the signal power equivalent at same distance. If we look at the red part of our contour, which is the footprint, we can find that in different directions, the contour belongs to different W-M circles. So in these directions the signal powers are determined by the path-loss exponent of their own W-M circles in our footprint model. Thus if we want to predict the signal power of some point, we should use the path-loss exponent of the direction this point located at.

In Fig. 28, we can generally separate the footprint into two parts, left and right. The left part is mostly covered by the W-M circle for the direction of 11.25°, while on the right the footprint is mostly covered by the circle for the direction of 168.75°. So we specifically use the path-loss exponents of these two directions to determine the signal strength on two sides of the footprint, which are 1.765 for the left and 1.333 for the right.

For each part, we calculate the average value of the signal powers we measured at $1m$ in directions belonging to this part and set this average value as the reference signal power P_0 of this part. From table 2, we get the average value of 39.48 for the left and 40.1 for the right part. Thus we can predict the signal powers of all locations for this scenario in both parts based on their own path-loss exponent and reference signal power. Having the predicted values of all locations, comparing them with the real data we collected, we can decide the error of our W-M footprint model for each location by the following equation:

$$Error = \frac{\left|\hat{P} - P\right|}{P}$$

where $\hat{P}$ represents the predicted value and P represents the real data we collected.

We use the same equation to quantify the errors of disc model. The average value of all path-loss exponents in Table 3 was used, which is 2.0605. We set the average value of all the data we collected at $1m$ as the reference signal power. Table 4 illustrates the errors of two models. We can find that except for directions of 0° and 180°, the errors of W-M model are smaller than disc model. So is the average error.

Table 4. (a) Error of two models for Scenario I

		Scenario I: Error (%)										
		Angle (Degree)										
		0	**5.625**	**11.25**	**16.875**	**22.5**	**33.75**	**45**	**56.25**	**67.5**	**90**	**112.5**
Model	**W-M**	7.38	5.87	4.75	4.45	5.22	3.82	4.13	9.35	4.98	4.05	3.77
	Disc	5.78	9.39	9.36	7.31	9.79	6.58	7.31	12.21	7.22	6.3	6.44

Table 4. (b) Error of two models for Scenario I

		Scenario I: Error (%)								
		Angle (Degree)								
		123.8	135	146	157.5	163.1	168.75	174.38	180	Average
Model	W-M	8.21	5.11	2.84	4.83	5.82	5.26	5.73	12.02	**5.95**
	Disc	11.33	6.21	5.88	11.51	6.24	10.95	8.48	7.19	**8.25**

4.4 Scenario II

4.4.1 Application

Scenario II is illustrated in Fig. 29. 'T' is the transmitter, which is located at the middle of the corridor. The area is separated into 4 sections: I, II, III and IV, as shown in Fig. 29. In each section, directions are defined by degrees range from 0° to 90° clockwise. At the intersections of two continuous sections, directions are defined as both 0° and 90°. For example, the intersection line of section I and II is defined both as 90° of section I and as 0° of section II. 224 data points are collected in this scenario at cross points in Fig. 29. This scenario might be applicable to a mobile wireless device traveling through a corridor.

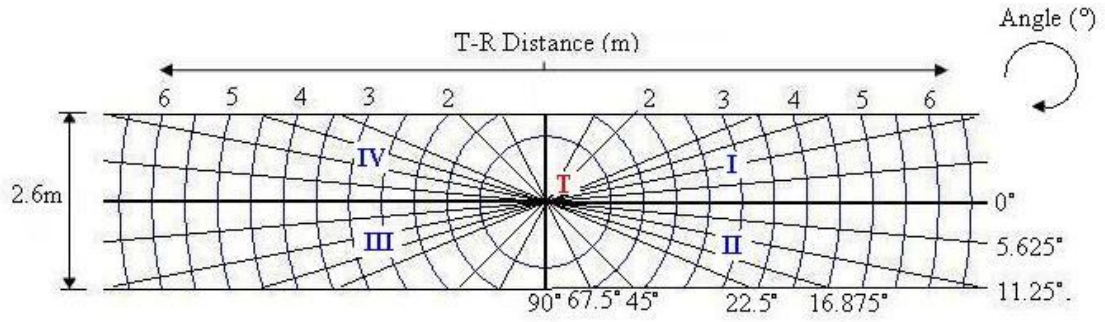

Figure 29. Measurement locations for Scenario II

4.4.2 Data

Table 5 contains the empirical data of Scenario II. The color map of this scenario is plotted in Fig. 30.

Table 5. (a) Data set for Scenario II

Scenario II: Measurement Data (-dBm)															
		Angle (Degree)													
			I							II					
		90(IV)/0(I)	22.5	45	67.5	73.125	78.75	84.375	90(I)/0(II)	5.625	11.25	16.875	22.5	45	67.5
T-R Distance (m)	1	36.6	37.2	37.2	37.6	40.6	39.9	39.7	40	42.6	39.8	38.4	39.2	40.1	37.4
	1.5			41.7	41.8	39.9	43	42.4	42.6	41.4	41.1	41.5	43	38.7	
	2				49.6	45	48.8	48.8	42.6	42.4	45.2	43.9	45.1		
	2.5				58.4	43.3	48.8	48.5	49.4	47	45.9	47.5	44.8		
	3				46.8	44.2	49.5	53.3	48.5	44.8	50.3	45.7	44.3		
	3.5					48.8	51.7	54.5	52.5	47.5	54	45.4			
	4					48.5	54.1	47	50.1	49	46.5	46.7			
	4.5						50.2	52.3	58.8	50.5	48.5				
	5						52.9	50.2	47.8	49.8	64.6				
	5.5						61	53.9	65.3	54.8	49.9				
	6						53.5	51.7	49.2	54.1	52.3				
	6.5						50.5	56.9	54.5	53.8	53.9				
	7							55	50	59.1					
	7.5							49.8	53.9	50.2					
	8							51.8	61.8	51.5					
	8.5							54.1	55.4	49.5					
	9							55.5	57.7	63.7					
	9.5							49.1	49.9	56.1					
	10							50	49.1	49.9					

Table 5. (b) Data set for Scenario II

	Scenario II: Measurement Data (-dBm)													
	Angle (Degree)													
		III							IV					
	90(II)/0(III)	23	45	67.5	73.13	78.75	84	90(III)/0(IV)	5.625	11.25	16.9	23	45	67.5
T-R Distance (m)	38.3	37.5	41.3	38.5	37.4	39.2	38.7	38.8	36.7	40	38.4	36.6	37.1	40.2
			38.6	42.2	40.7	40.1	45.2	42	41.4	39.5	40.1	39.9	40.9	
				41.1	44.2	43.8	44.9	42.9	51.2	51.9	42.3	44.9		
				50.5	45.4	45.1	47.6	43.9	41.8	49.9	43.5	47.3		
				50.2	58.9	49.9	44.9	47.4	45.4	54.3	44.8	45.1		
					46.5	47.8	42.5	45.5	49.7	48.6	49.5			
					51.6	49	48.2	44.4	47.2	50.1	51.1			
						60.1	57.4	47.8	44.2	51.1				
						49.9	54.5	49.9	52.4	50.6				
						53.9	56.2	53.3	49.4	59.7				
						56.8	50.3	55.1	47.6	60.2				
						52	56.7	66.1	64.5	52				
							52.9	56.5	54.1					
							59.7	52.9	51.1					
							52.4	50.7	48					
							56.2	58.4	55					
							64.8	68	56.8					
							54.4	54.8	58.2					
							53.8	58.5	50.8					

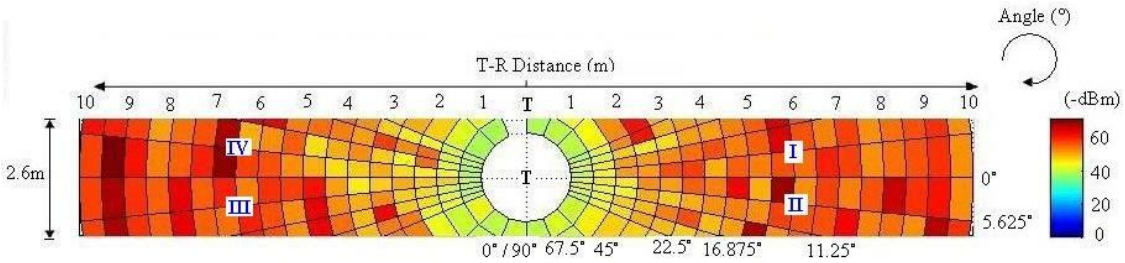

Figure 30. Color map for Scenario II

4.4.3 Analysis

We use n and σ to characterize the data collected in this scenario. In Fig. 31, data in Table 5 are fit into straight lines and n are calculated out for directions, which have more

than 12 data points. n, σ and their average values are shown in Table 6 and plotted in Fig. 32.

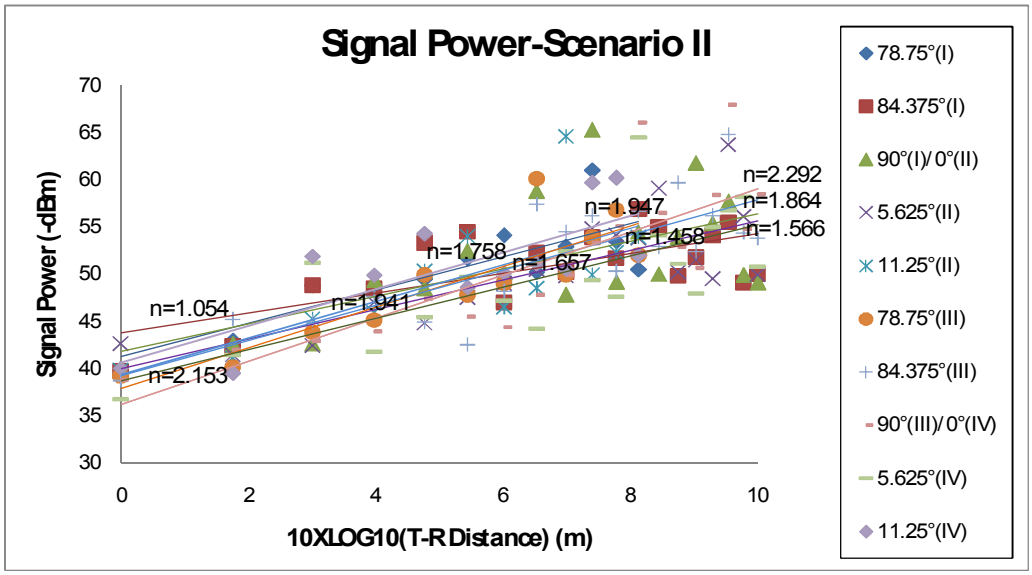

Figure 31. Signal Power v.s. T-R distance (Scenario II)

Table 6. (a) Shadowing coefficient (σ) and path loss exponent (n) for Scenario II

Section	I			II	
Direction	1	2	3	4	5
Angle (°)	78.75	84.375	90°/0	5.625	11.25
n	1.758	1.054	1.458	1.566	1.941
σ	2.880	3.141	4.886	3.472	4.253

Table 6. (b) Shadowing coefficient (σ) and path loss exponent (n) of scenario II

Section	III			IV		Average
Direction	6	7	8	9	10	
Angle (°)	78.75	84.375	90/0	5.625	11.25	
n	2.153	1.864	2.292	1.657	1.947	1.769
σ	3.012	3.715	4.293	4.366	3.739	3.776

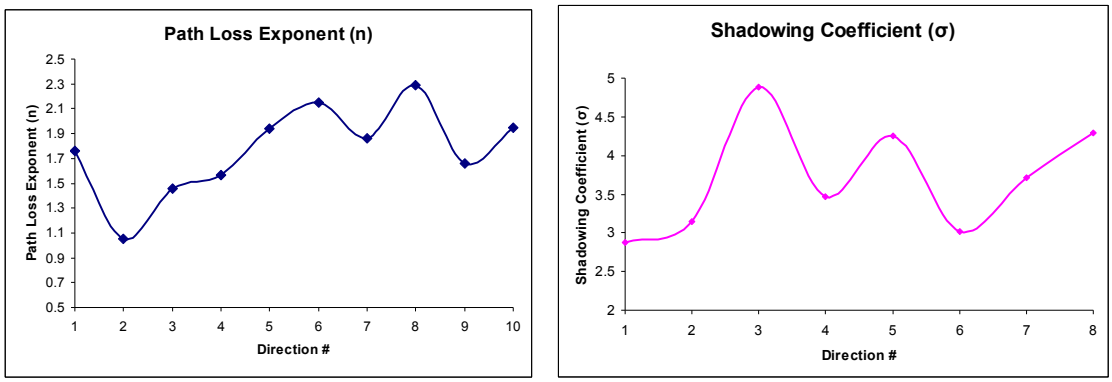

Figure 32. *n* and σ distribution for Scenario II

In Fig. 32, we do not find similar trend of curves in Fig. 27. Considering that in this scenario the transmitter is set at the middle of hall way, there is no direction along the wall, which can be the reason of our failure finding similar trend.

4.4.4 W-M Footprint

The logarithmic W-M footprint of Scenario II is plotted in Fig. 33. The circles on the right side of the transmitter are generally bigger than the left ones, which is caused by the fact that *n* is larger at left. The environment of the hall way was not symmetric enough. For example, the construction materials are different. Since that the number of rooms, doors, windows and the area of walls are different on two sides of the hall way and they are of different materials, they would add various influences on signal propagation. Moreover, the transmitter was not located at the middle of the whole hall way. It is closer to the left end (the side of Section III and IV in Fig. 29). All of these can lead *n* into different values on the left and right side. Thus, the footprints on the left and right are not

same. However we can still find some symmetry in the shape of the footprint. These are just what we expect.

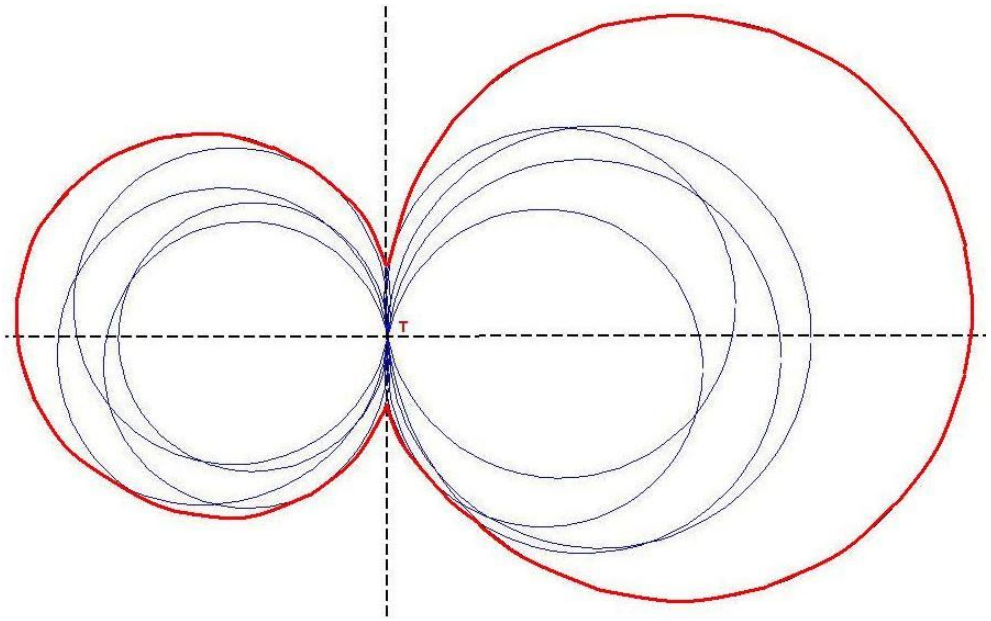

Figure 33. W-M footprint for Scenario II in logarithmic scale

Like what we did for Scenario I, we compare the errors of our W-M model and disc model. We still use the average value of n and average value of data at $1m$ to calculate the errors of disc model. The footprint for the scenario can also be separated into left ans right parts. The right part of our W-M footprint is dominant by circle for the direction of 84.375° in section I. The left part consists of 3 circles. However, to simplify the calculation, we only use the circle for direction of 5.625° in section IV. The errors for this scenario are listed in Table 7.

Table 7. (a) Error of two models for Scenario II

Scenario II: Error (%)															
		Angle (Degree)													
			I							II					
		90(IV)/0(I)	22.5	45	67.5	73.125	78.75	84.375	90(I)/0(II)	5.625	11.25	16.875	22.5	45	67.5
Model	W-M	6.61	4.89	3.43	10.56	3.98	11.19	9.02	9.91	8.08	9.01	3.42	3.19	4.16	4.33
	Disc	5.87	4.17	2.28	7.36	3.83	5.57	5.82	6.82	5.16	5.03	3.06	2.96	5.57	3.61

Table 7. (b) Error of two models for Scenario II

Scenario II: Error (%)																
		Angle (Degree)														
			III							IV						Average
		90(II)/0(III)	22.5	45	67.5	73.125	78.75	84.375	90(III)/0(IV)	5.625	11.25	16.875	22.5	45	67.5	
Model	W-M	0.47	2.61	7.04	5.21	5.21	4.04	5.93	5.53	6.42	7.42	3.23	3.93	2.47	4.28	5.56
	Disc	1.17	3.33	7.32	4.8	5.11	3.95	5.82	5.53	6.77	6.5	3.67	4.09	3.4	3.61	4.72

In Table 7, we can find that for Scenario II, the average error of disc model is lower than W-M footprint. This might caused by the fact that we use the path-loss exponent for the direction of 84.375° in section I for our error calculation of the right part W-M footprint. This direction has much smaller *n* than other directions on the same side. We can see in Fig. 33, the largest circle on the right is much bigger than the other circles on the right. Table 7 (a), which represents the errors of the right side, gives larger errors of W-M model. This small *n* might be caused by errors during our measurement. However, on average W-M only is only worse than disc model by 0.84%, which is quite small.

4.5 Scenario III

4.5.1 Application

In Scenario III, the transmitter 'T' is located at the corner of the hall way. 193 data points are collected in 13 directions range from 0° to 90°, as shown in the Fig. 34 as the cross points. If a sensor node is deployed at a corner of corridors, we can use this scenario to analyze the footprint of it.

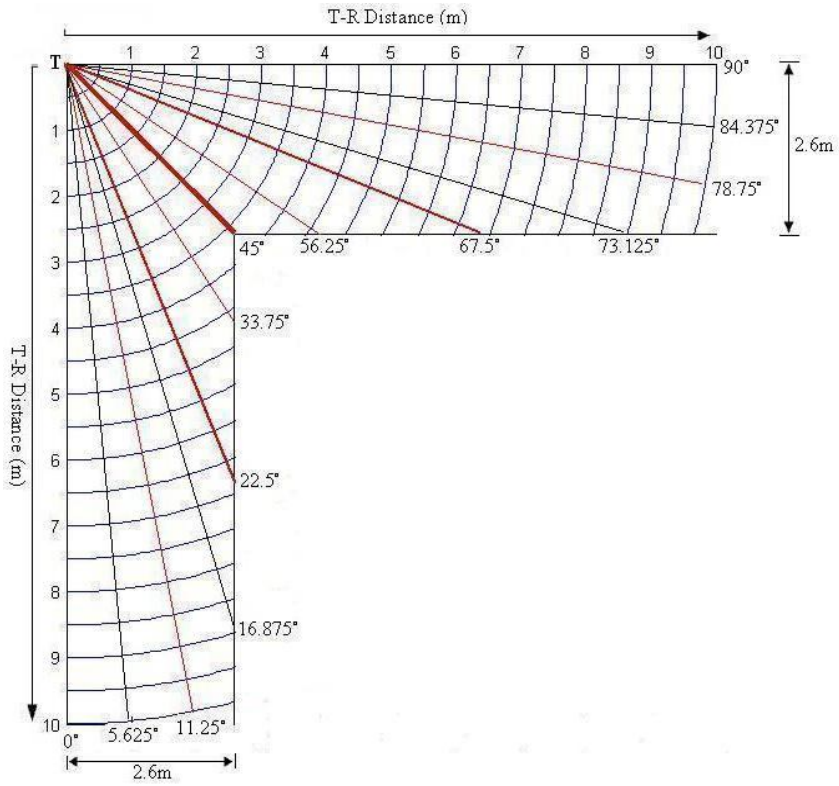

Figure 34. Measurement locations for Scenario III

4.5.2 Data

Table 8. Data set for Scenario III

Scenario III: Measurement Data (-dBm)													
		Angle (Degree)											
		0	5.625	11.25	16.875	22.5	33.75	45	56.25	67.5	73.125	78.75	84.375	90
T-R Distance (m)	1	43.9	44.6	45.2	43.4	41.5	40.1	42.3	42.4	59.6	53.4	47.2	43	38.7
	1.5	39.7	41.2	42.6	44.8	47	44.9	39.8	57	64.3	54.5	44.7	42.8	40.9
	2	41.5	42.9	44.3	44.5	44.6	53.8	42.7	48.9	77	64.35	51.7	50.5	49.2
	2.5	46.6	46.6	46.6	45	43.4	56.3	43.1	47.8	44.3	48.1	51.8	54.3	56.8
	3	49.8	49.9	50	49.75	49.5	59.1	54.2	58.5	48.2	51.5	54.8	54.2	53.5
	3.5	52.9	49.6	46.3	46.3	46.3	51.3		51	50.3	53.2	56	57.8	59.6
	4	59.4	50.8	50.4	50.5	48.9	51.4		50.9	54	52	47.7	51.6	55.6
	4.5	54.3	50.3	50.2	48.5	52.1	50.2		54.8	52.1	48.9	56.2	55.4	63.1
	5	55.3	56.5	46.7	49.4	47.9	48		49.9	51.7	57.4	49.4	67.5	64.8
	5.5	51.8	63	49.3	53.6	60.7				57.2	60.6	53.7	68.5	63.1
	6	58.8	52.6	50.8	55.5	53.7				63.2	54.8	60.4	65.6	60.6
	6.5	59.2	50.45	54.7	56	54.7				60.5	58.3	66.7	58.2	67.6
	7	54.2	52.1	56.3	55						54.2	57.9	61.5	60.9
	7.5	67.7	53.6	54.6	54.5						59.3	60	60.5	54.8
	8	60.7	51.5	52.5	59.7						57.3	64.9	61.5	59.1
	8.5	59.5	51.9	57.4	45.5						56.8	58.5	61.5	59.5
	9	56.9	55.6	50.9								55.5	58.4	64.3
	9.5	68.1	55.5	53								60.8	68.2	64.2
	10	67.2	58.3	54.8								66.4	61.5	63.7

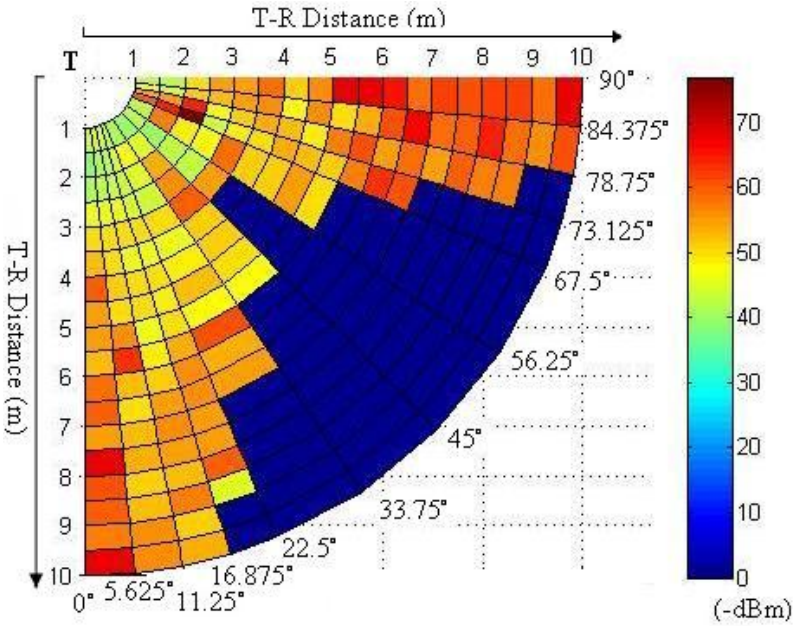

Figure 35. Color map for Scenario III

We list the data collected from Scenario III in table 8 and plot the color map in Fig. 35. So we can read the signal power more clearly.

4.5.3 Analysis

Like the other two scenarios, n and σ are used to analyze the data for this scenario as shown in Fig. 36, Table 9 and Fig. 37 to give us a basic idea about the propagation environment, where the empirical data are held. Like Fig. 27, in Fig. 37, we can find that the path loss exponents are higher at two ends of the curves, which represent the places close to the wall.

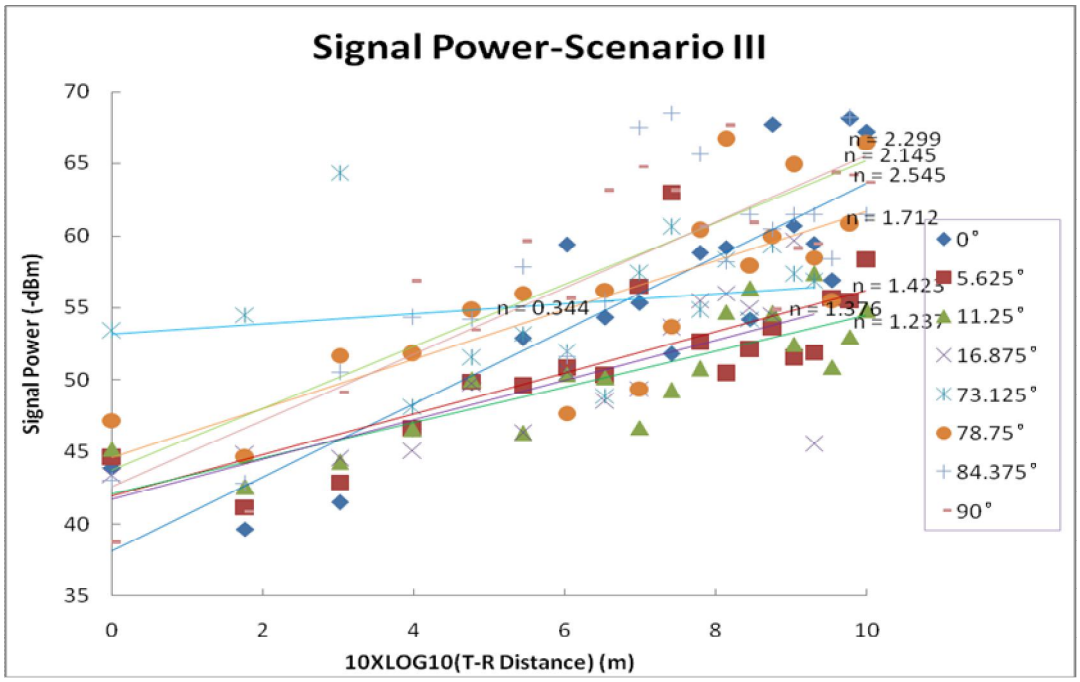

Figure 36. Signal power vs. T-R distance (Scenario III)

Table 9. Shadowing coefficient (σ) and path loss exponent (n) for Scenario III

Angle (°)	0	5.625	11.25	16.875	73.125	78.75	84.375	90	Aver-
Direction	1	2	3	4	5	6	7	8	age
n	2.545	1.423	1.237	1.376	0.344	1.712	2.145	2.299	1.635
σ	3.785	3.294	2.221	3.218	4.035	3.928	4.278	4.401	3.645

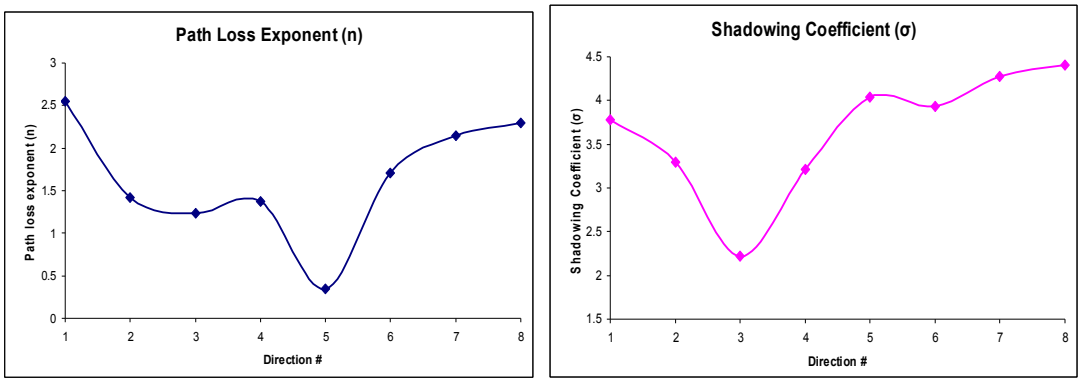

Figure 37. n and σ distribution for Scenario III

4.5.4 W-M Footprint

In this scenario, the transmitter is at the corner. The logarithmic footprint built is shown in Fig. 38. Generally directions closer to vertical line have larger W-M circles than directions closer to horizontal lines, which reflects n calculated by the empirical data in these directions. We can find that the footprint has two trends. One goes right and the other goes down. These are just directions along the wall. So these trends are reasonable in this scenario with transmitter at the corner. If we use disc model, these trends will not be reflected. Table 10 shows the errors of W-M footprint model in Fig. 38 and footprint built by disc model. Even though, we still see errors of our W-M footprint, in most of the

directions, W-M footprint reflects smaller errors than disc model. On average, W-M footprint is better than disc model as well.

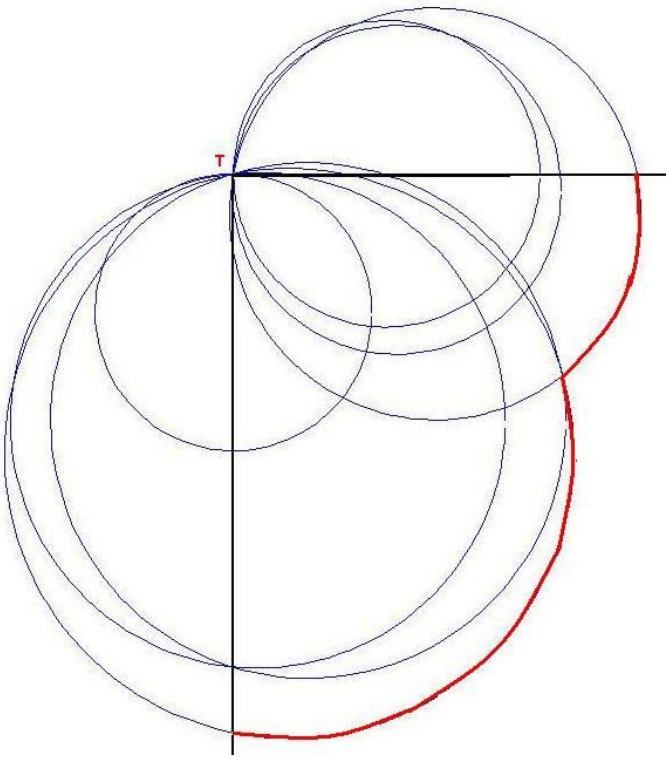

Figure 38. W-M footprint for Scenario III in logarithmic scale

Table 10. Error of two models for Scenario III

Scenario III: Error (%)															
		Angle (Degree)													
		0	5.625	11.25	16.875	22.5	33.75	45	56.25	67.5	73.125	78.75	84.375	90	Average
Model	W-M	9.02	4.23	1.96	4.92	5.26	7.49	8.96	6.38	14.83	10.79	8.35	7.26	7.49	7.46
	Disc	7.22	10.12	11.22	10.05	10.1	9.51	13.17	7.78	12.36	7.02	5.56	5.78	7.22	9.01

4.6 Conclusion

In this chapter, we introduce the test set up and describe three scenarios specifically. The empirical data we collected in these scenarios are listed and plotted into color map to give a clear representation. We calculate out the path-loss exponents and shadowing coefficients of directions in each scenario. After that, a W-M footprint consisting of overlapping W-M circles is built for each scenario based on the n, which determines the radius of W-M circle in each direction. Then we calculate the errors of our W-M footprint and compare with disc model. Even though W-M footprints we built are not perfect, generally it is better than the disc model. Analyses of the footprint in this chapter and previous chapters are focusing on single node. We will go up to the system level and analyze the network connectivity in the next chapter.

CHAPTER 5

CONNECTIVITY ANALYSIS FOR RANDOMLY DEPLOYED NETWORKS IN SHADOWING ENVIRONMENTS

5.1 Introduction

In the earlier chapters we investigated a means to improve the modeling of communication footprints for individual nodes. In this chapter we move to the system level and focus on the connectivity between nodes randomly deployed to form networks. Better analysis of the network connectivity will provide useful information for the improvement of network reliability, which is a key issue in wireless sensor networks. Graph theory is used to analyze these networks. Some relative definitions in graph theory are introduced first. Then connectivity in wireless sensor networks is specified. After that, we present an algorithm to analyze the connectivity of randomly deployed networks and discuss the results from its use.

5.2 Connectivity

5.2.1 Connectivity in Graph Theory

Graph Theory is a specific area of mathematics focusing on the study of graphs. Before we take advantage of the graph theory to analyze the connectivity of wireless sensor networks, some relevant terms will be first defined. From graph theory [16], a

graph G is a triple consisting of a **vertex set** $V(G)$, an **edge set** $E(G)$ and a relation that associates with each edge two vertices called its **endpoints**.

Graph may exhibit two kinds of **connectivity: Connectivity** and **Edge-connectivity**, which are defined as follows: [16]

- **Connectivity** of Graph G: the minimum size, k, of a vertex set S such that G-S is disconnected or has only one vertex. A graph is ***k*-connected** if its connectivity is at least k.
- **Edge-connectivity** of Graph G with at least two vertices: the minimum size of a **disconnecting set** (a set $F \subseteq E(G)$ such that G-F has more than one component). A graph has at least two vertices is ***k*-edge-connected** if every disconnecting set has at least k edges.

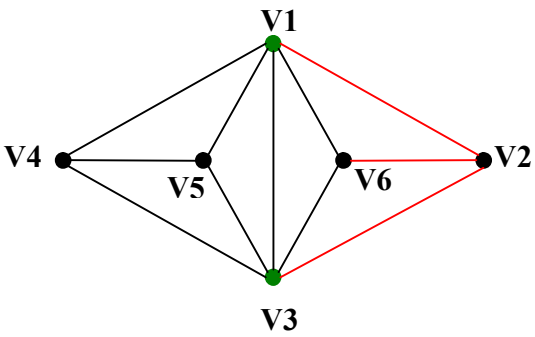

(b) Graph A:
Vertex connectivity=2,
Edge connectivity=3.

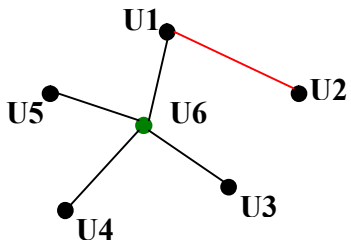

(a) Graph B:
Vertex connectivity=1,
Edge connectivity=1.

Figure 39. Example graphs

To better understand these terminologies, two graphs are shown in Fig. 39 as examples. Graph A has a vertex set $V(A) = \{V1, V2, ..., V6\}$ and an edge set

$E(A) = \{V1V2, V1V3, V1V4, ...\}$ of size 11; Graph B has a vertex set $V(B) = \{U1, U2, ..., U6\}$ and an edge set $E(B) = \{U1U2, U1U6, U3U6, U4U6, U5U6\}$.

Edges are represented by their endpoints. For example, an edge connecting vertices *V1* and *V2* is called edge *V1V2*. Graph *B* is 1-connected, since that if we delete one vertex, like *U6* or *U1*, the graph is no-longer connected. In Graph *A*, no matter which vertex is deleted the graph is still connected. If we want to disconnect *A*, the minimal size of the vertex set, *S*, to be deleted from $V(A)$ is two. For example, by removing vertices *V1* and *V2* the graph is disconnected. To determine the edge-connectivity of graphs, we should focus on edge sets. In Graph *B*, discarding only one edge can make it disconnected, such as *U1U2*. Graph *B* has the same edge connectivity as vertex connectivity. However, this is not always true. For Graph *A*, as discussed above, the vertex connectivity is two, but deleting two edges cannot disconnect the graph. The minimal size of disconnecting edge set, *F*, is three. One example set is $F = \{V1V2, V2V6, V2V3\}$.

Graph theory presents another definition for connectivity: A graph *G* is **connected** if it has a *u,v*-path whenever $u, v \in V(G)$ (otherwise, *G* is **disconnected**). So here *G* is connected means *G* is 1-edge-connected and this definition can be served as another definition of **1-edge-connectivity**. For example, if in Fig. 39 (b), whichever pair of vertices we choose, a path can be found. Pair $\{U2, U4\}$ has a path $\{U2U1, U1U6, U6U4\}$; pair $\{U2, U5\}$ has a path $\{U2U1, U1U6, U6U5\}$; etc. So, Graph B is connected.

Below we present some other definitions important for the content in this chapter. These concepts are illustrated using Fig. 39 and 40.

- When *u* and *v* are the endpoints of an edge, they are **adjacent** or are **neighbors**.
- **Weighted graph**: a graph with numerical labels on the edges.
- **Complete graph**: simple graph in which each two vertices are adjacent.
- **Subgraph** (of graph *G*): a graph whose vertices and edges all belong to *G*.
- **Spanning subgraph**: a subgraph containing each vertex.
- **Cycle**: a graph with an equal number of vertices and edges whose vertices can be placed around a circle so that two vertices are adjacent if and only if they appear consecutively along the circle.
- **Spanning tree**: a spanning, connected, acyclic subgraph.
- **Minimum spanning tree**: spanning tree with minimum sum of edge weights.
- **Component**: maximal connected subgraph. So a connected graph has only component, which is itself.

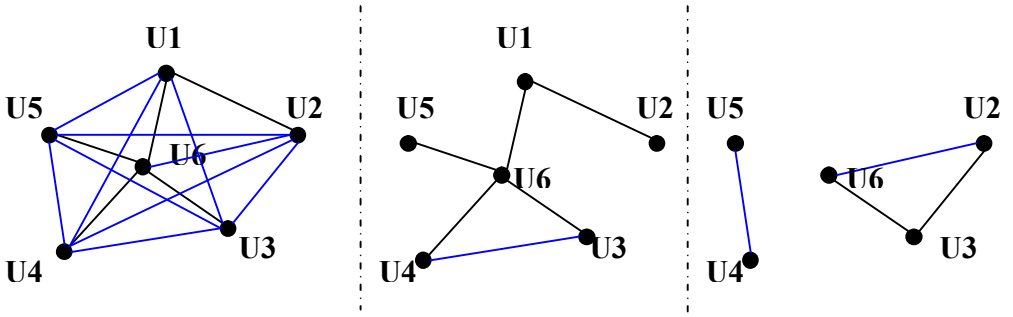

(a) Complete graph **(b) Spanning subgraph** **(c) Subgraph (2 components)**

Figure 40. Example complete graph and subgraphs

Fig. 40 (a) gives an example of a complete graph, which is constructed by adding edges to graph *B* in Fig. 39 (b) until each vertex connects with every other. Since all

vertices and edges of Fig. 40 (b), (c) and Graph *B* in Fig. 39 (b) belong to the complete graph shown in Fig. 40 (a), they are subgraphs of it. Among these subgraphs, Fig. 40 (c) has two components which consist specifically with vertex set $\{U4, U5\}$ and $\{U2, U3, U6\}$. On the other hand, Fig. 40 (b) and Graph *B* have only one component and have the same vertex set as Fig. 40 (a), so they are spanning subgraph. Meanwhile, graph *B* has no cycles, so it is also a spanning tree. However, Fig. 40 (b) has a cycle $\{U3U4, U4U6, U6U3\}$, thus it is not a spanning tree. A weighted graph can be built, if we add a weight to each edge. Then we can find a minimum spanning tree of the graph.

5.2.2 Connectivity in a Wireless Sensor Network

What we are concerned with in wireless sensor networks is **edge-connectivity**, that is, is there a communication link (an edge) between two sensor nodes (vertices). To illustrate the use of graph theory, we assume in this chapter that our sensor network consists of a number of nodes randomly deployed (with a uniform distribution) over a surface. We will use graph theory methods to find the relationship between the connectivity of this sensor network and several parameters (e.g., density of nodes, path-loss exponent, and variability in path-loss).

5.2.3 Randomness in the Network Model

A uniform distribution over some range $[a, b]$ means that any value within the range has equal probability. The probability density function (pdf), $f(x)$, and cumulative

density function (cdf), $F(x)$, of the uniform distribution are listed as follows (See Fig. 41):

$$f(x)=\begin{cases}\dfrac{1}{b-a} & \text{for } a \le x \le b \\ 0 & \text{for } x > a \text{ or } x < b\end{cases} \qquad F(x)=\begin{cases}0 & \text{for } x < a \\ \dfrac{x-a}{b-a} & \text{for } a \le x \le b \\ 1 & \text{for } x > b\end{cases}$$

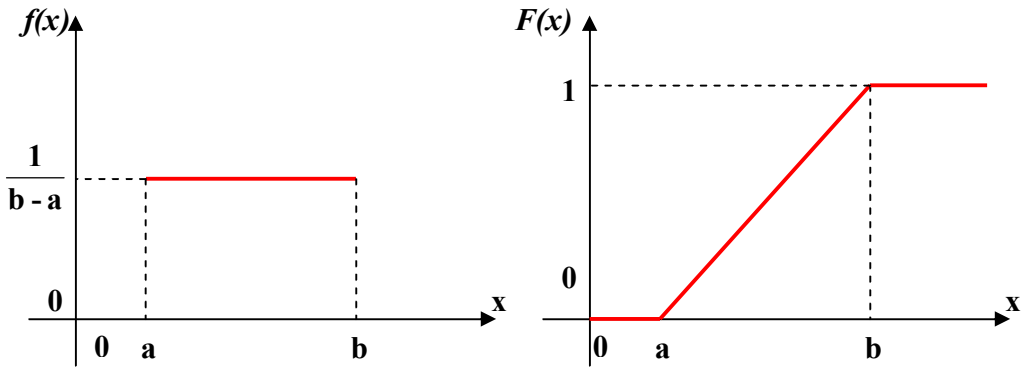

Figure 41. pdf curve and cdf curve of Uniform Distribution

In our case, nodes are uniformly distributed over a plane. The locations of the nodes depend on both x and y coordinators. So both these values will be uniformly distributed in two dimensions. For example, if nodes are deployed over an area $A \times B$, x-coordinators will be uniformly distributed over $[0, A]$ and y-coordinators will be uniformly distributed over $[0, B]$. Thus the locations of the nodes follow the joint pdf and cdf of uniform distribution. The joint pdf for an area of $a \le x \le b, c \le y \le d$ is (See Fig. 42):

$$f(x,y)=\begin{cases}\dfrac{1}{(b-a)(d-c)} & \text{for } a \le x \le b, c \le y \le d \\ 0 & \text{others}\end{cases}$$

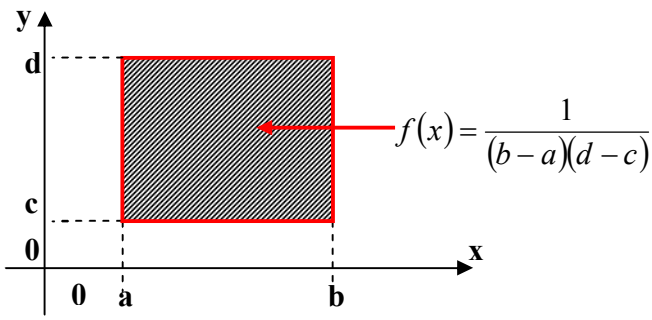

Figure 42. Joint pdf of uniform distribution.

The joint cdf for an area of $a \le x \le b, c \le y \le d$ is (See Fig. 43):

$$F(x,y)=\int_{-\infty}^{x}\int_{-\infty}^{y} f(x,y)\cdot dudv$$

$$=\begin{cases} 0 & \text{for } x < a \text{ or } y < c \\ \dfrac{(x-a)(y-c)}{(b-a)(d-c)} & \text{for } a \le x \le b, c \le y \le d \\ \dfrac{x-a}{b-a} & \text{for } a \le x \le b, y > d \\ \dfrac{y-c}{d-c} & \text{for } x > b, c \le y \le d \\ 1 & \text{for } x > b, y > d \end{cases}$$

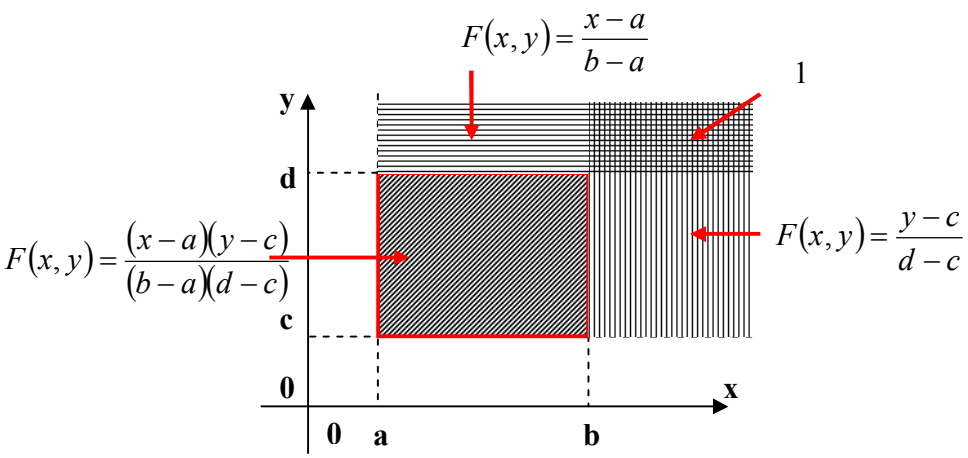

Figure 43. Joint cdf of uniform distribution.

Besides the locations of nodes, another random variable, which is the variability in path-loss, is also include in our scenario. However, this random variable has Gaussian distribution (per the log-normal shadowing model) and will impact the link reliability (i.e. probability of edge connectivity).

5.2.4 Building Graph and Connectivity Probability Matrix

Fig. 44 shows 30 nodes deployed within a $20\,m \times 20\,m$ area. In order to better analyze the random networks by graph theory, we build a graph and a matrix to represent a random network. Thus we can analyze the connectivity and try to improve the reliability of the network by the graph and matrix.

A weighted graph is built where vertices represent the nodes and edges represent the connections between nodes. If two nodes can communicate with each other, they are *neighbors* in the graph. In the graph, each edge has a weight which is the probability of the corresponding pair of nodes being able to communicate with each other. As discussed in Section 2.3, the probability is influenced by n, d, σ (See 2.3).

Using the probability for all links, a $N \times N$ symmetric matrix (N—number of nodes/vertices) is built based on the graph. In the matrix, every column and row represents one of N nodes i. And the value of (i, j) is the probability of connection between node i and j. We call this matrix the 'Connectivity Probability Matrix' for the network shown in Fig. 44, a subset of connectivity probability matrix is given in Table 11. This table is only for a subset of Nodes 1 through 5, the complete connectivity probability matrix for 30 nodes in Fig. 44 can be found in Appendix A.

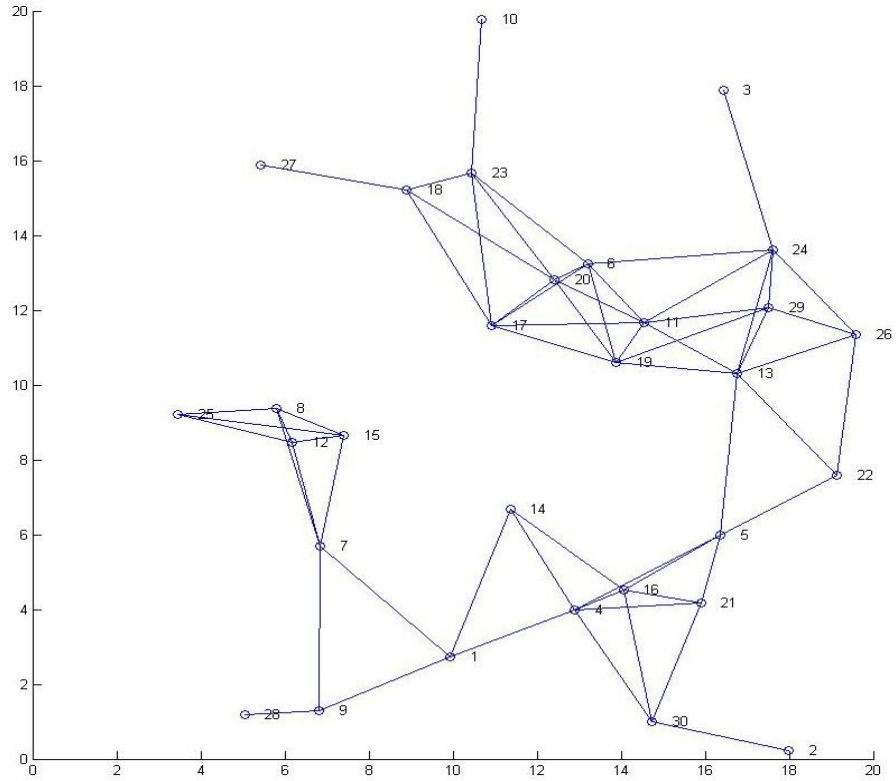

Figure 44. Random node deployment graph for $N = 30$, $n = 3$, $\sigma = 3$ (Minimal $k = 1$ connectivity probability of this graph is 0.99992)

Our objective now is to understand the probability that our network will be connected. This probability is dependent on the "weakest link" in the graph, that is the edge which has the highest probability and when removed disconnects the graph. Based on the graph and connectivity probability matrix, the threshold of link reliability, which can provide the 1-connectivity of the network, can be decided.

Table 11. Connectivity probability matrix example

Connectivity Probability Matrix					
Node	**1**	**2**	**3**	**4**	**5**
1	1	0.031317	8×10^{-15}	1	0.315355
2	0.031317	1	0	0.73997	0.874972
3	8×10^{-15}	0	1	5.14×10^{-11}	6.27×10^{-7}
4	1	0.73997	5.14×10^{-11}	1	0.999998
5	0.315355	0.874972	6.27×10^{-7}	0.999998	1

5.3 Simulation

In order to better understand the connectivity of randomly deployed networks, the minimal link reliabilities with various N, n and σ need to be analyzed. Considering that the number of nodes can be very large and that the locations of the nodes are random, a routine was developed to simulate different scenarios. In our simulation, we can vary the parameters (N, n, σ) of the network by changing the corresponding variables in the routine.

5.3.1 Kruskal's Algorithm

Based on the graphs we build, the reliability of networks becomes equivalent to the connectivity of the graph. Using graph theory vernacular, our objective can be translated into finding a spanning subgraph with maximum weight (i.e., a spanning subgraph with maximum sum of edge-weight). Kruskal's algorithm aims at finding the minimum

spanning tree. If we change the probability of each link to its complement of 1, our goal will become finding a minimum spanning subgraph, the objective of Kruskal's algorithm. The only difference is that cycles do not harm in our objective, so we can accept a spanning subgraph, and not require a tree.

Kruskal's algorithm can be summarized as follows: [16]

Kruskal's Algorithm

Input: A weighted connected graph (such as Fig. 44)

Idea: Maintain an acyclic spanning subgraph *H*, enlarging it by edges with low weight to form a spanning tree. Consider edges in non-decreasing order of weight, breaking ties arbitrarily.

Initialization: Set $E(H)=\emptyset$

Iteration: If the next cheapest edge has end points in two separate components of *H*, then include it; otherwise, discard it. Terminate when *H* is connected.

Considering that cycles do no harm in our case, we do not need to confirm it is a tree. So the step of checking if the lightest edge has end points in two separate components can be omitted. We directly include the lightest edge at each iteration. However, we still regard the probability of each link as the weight. So what we try to find is the maximum spanning subgraph not minimum. Thus our modified Kruskal's algorithm is as follows:

Modified Kruskal's Algorithm

Input: A weighted complete graph

Idea: Maintain a spanning subgraph H, enlarging it by edges with high weight to form a connected spanning subgraph. Consider edges in decreasing order of weight.

Initialization: Set $E(H)=\emptyset$

Iteration: Include the next heaviest edge at edge step. Terminate when H is connected.

Based on this algorithm, a Matlab program was developed to fulfill the goal (included in attached CD). The flow chart for this routine is presented in Fig. 45. The basic idea of the program is that at each iteration search the next largest value in the connectivity probability matrix, add this edge/link to the subgraph/network, and then check if the subgraph/network is connected. The key point in this program is checking the connectivity of the subgraph/network. The method used was counting the remaining components of the subgraph as edges continuously added in. So when the number of remaining components equals one, the spanning subgraph is connected.

To track the number of components, a matrix, $\boldsymbol{C}$, is built, which represents the components of the graph. Also, a variable m is defined, to keep track of the number of components. In $\boldsymbol{C}$, each column represents a component, and nodes included in this component are listed as values in this column. So the number of non-empty columns is the number of components, m. If we have a connected graph, $\boldsymbol{C}$ should include one column with all nodes and all the other columns are empty. (i.e., m will equal to 1.)

At each iteration, an edge is added to the subgraph, and $\boldsymbol{C}$ is searched to find the adjacent vertices of it. For example, edge uv with adjacent vertices u and v. If u and v are in the same column, the process ends. If they are not in the same column, assume that

search ***C*** and find out that u is in column i, and v is in column j. At the end of this process uv will combine components i and j. Vertices in these components will be in the same component. Thus we add all values in column j to column i, and set column j to be all zeros (Decreasing m by 1). If m equals 1, the maximum value found in this iteration is the probability of the weakest link we need to confirm $k = 1$ connectivity.

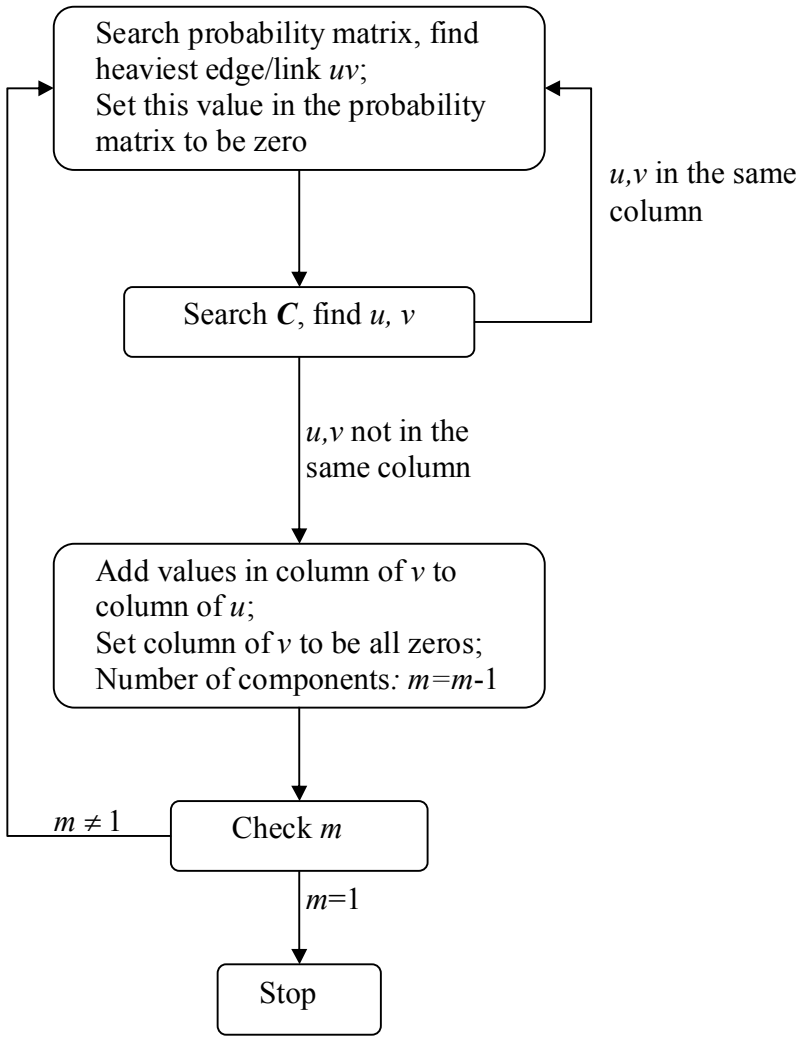

Figure 45. Flow chart of the modified Kruskal's algorithm

5.3.2 Example of the modified Kruskal's Algorithm

To better understand the algorithm, an example is illustrated in this section. We begin with a connectivity probability matrix, ***P***, for a 5 node network. Fig. 46 shows the initialized graph, which has five isolated vertices and no edges.

Table 12. Initialized connectivity probability matrix

Connectivity Probability Matrix, *P*					
Node	**1**	**2**	**3**	**4**	**5**
1	1	0.029103	0.999909	0.002468	0.991689
2	0.029103	1	0.999924	0.559533	1
3	0.999909	0.999924	1	0.909933	1
4	0.002468	0.559533	0.909933	1	0.601714
5	0.991689	1	1	0.601714	1

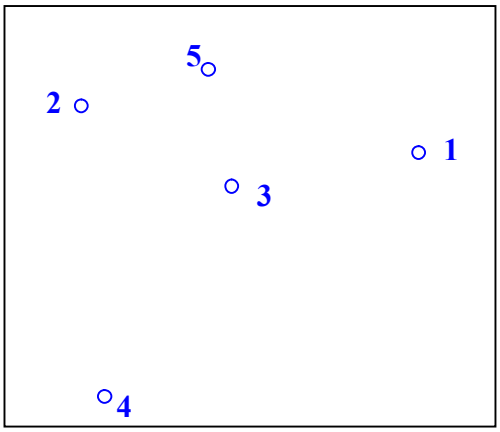

Figure 46. Initialized graph

Initialization of the component matrix, ***C*** is as Table 13. Since no edges are included in the subgraph now, graph consists of five isolated nodes, each being a component. So in Table 13, five non-empty columns exist, each of which has a non-zero value representing

the node included in this component. That is the number of components (i.e., non-empty columns): $m=5$

Table 13. Initialized component matrix

Components Matrix, *C*				
1	**2**	**3**	**4**	**5**
0	0	0	0	0
0	0	0	0	0
0	0	0	0	0
0	0	0	0	0

In the following iterations, numbers colored red in the matrixes are updated values in the current and previous iterations. If the connectivity probability matrix has more than one equal maximum value in current iteration, the first encountered when searching will be set as the maximum. Moreover, since ***P*** is symmetric, only the upper triangle part is searched to find the maximal value and updated.

The iterations are as follows:

Iteration 1:

- ***P***(2, 5) is found to be the largest value by searching through ***P***. This value in ***P*** represents the heaviest edge in the complete graph, i.e. strongest link in the network. (There are two values in *P* equal 1. ***P***(2, 5) is the first one by our searching order, so program will choose it as the largest one at this step.)
- We search through ***C*** to decide which columns (i.e. components) these two endpoints belong to. The result is that '2' is in column 2, '5' is in column 5. They are in different columns (i.e. components). So we combine these two columns to make them

one component in our updated matrix ***C***. The graph after the first iteration is shown in Fig. 47.

Table 14. Component matrix after 1st iteration

Components Matrix, *C*				
1	2	3	4	0
0	5	0	0	0
0	0	0	0	0
0	0	0	0	0
0	0	0	0	0

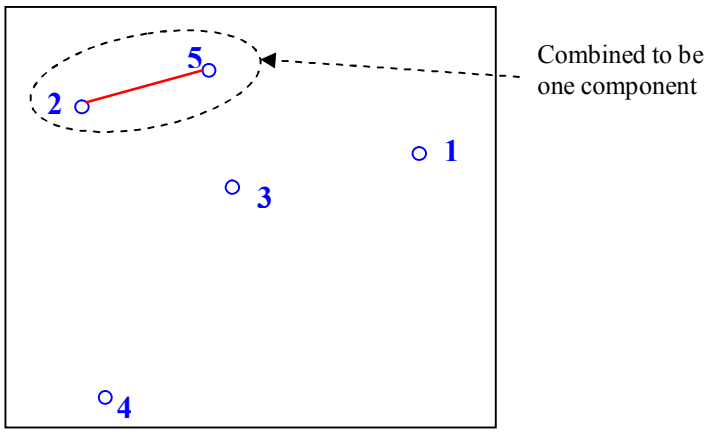

Figure 47. Graph after 1st iteration

- Decrease the number of components: $m = 5 - 1 = 4$
- Set $\boldsymbol{P}(2, 5) = 0$, since this edge has been considered in the current iteration.

The connectivity probability matrix, ***P*** after the first iteration now becomes:

Table 15. Connectivity probability matrix after 1st iteration

Connectivity Probability Matrix, *P*					
Node	**1**	**2**	**3**	**4**	**5**
1	1	0.029103	0.999909	0.002468	0.991689
2	0.029103	1	0.999924	0.559533	0
3	0.999909	0.999924	1	0.909933	1
4	0.002468	0.559533	0.909933	1	0.601714
5	0.991689	1	1	0.601714	1

Iteration 2:

- Search $\boldsymbol{P} \rightarrow$ The maximum value is $\boldsymbol{P}(3, 5) = 1$.
- Search $\boldsymbol{C} \rightarrow$ '3' and '5' are in different columns.
- Combine the columns that vertices '3' and '5' are in. $\rightarrow$ $m = 4 - 1 = 3$
- Set $\boldsymbol{P}(3, 5) = 0$.

Table 16. Component matrix after 2nd iteration

Components Matrix, *C*				
1	0	3	4	0
0	0	2	0	0
0	0	5	0	0
0	0	0	0	0
0	0	0	0	0

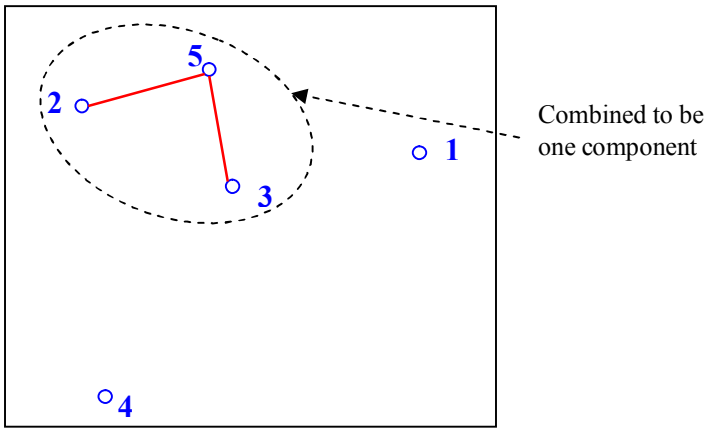

Figure 48. Graph after 2nd iteration

Table 17. Connectivity probability matrix after 2nd iteration

Connectivity Probability Matrix, *P*					
Node	**1**	**2**	**3**	**4**	**5**
1	1	0.029103	0.999909	0.002468	0.991689
2	0.029103	1	0.999924	0.559533	0
3	0.999909	0.999924	1	0.909933	0
4	0.002468	0.559533	0.909933	1	0.601714
5	0.991689	1	1	0.601714	1

Iteration 3:

- Search $\boldsymbol{P} \rightarrow$ Maximum value is $\boldsymbol{P}(2, 3) = 0.999924$.
- Search $\boldsymbol{C} \rightarrow$ '2' and '3' are in the same column, which means they are already connected and in the same component.
- Go on to the next iteration.
- Set $\boldsymbol{P}(2, 3) = 0$.

Table 18. Component matrix after 3rd iteration

Components Matrix, *C*				
1	0	3	4	0
0	0	2	0	0
0	0	5	0	0
0	0	0	0	0
0	0	0	0	0

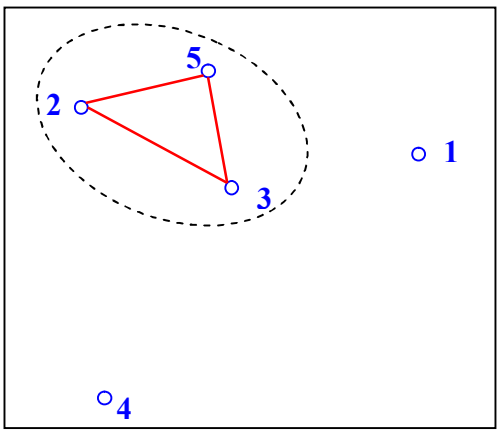

Figure 49. Graph after 3rd iteration

Table 19. Connectivity probability matrix after 3rd iteration

Connectivity Probability Matrix, *P*					
Node	**1**	**2**	**3**	**4**	**5**
1	1	0.029103	0.999909	0.002468	0.991689
2	0.029103	1	0	0.559533	0
3	0.999909	0.999924	1	0.909933	0
4	0.002468	0.559533	0.909933	1	0.601714
5	0.991689	1	1	0.601714	1

Iteration 4:

- Search $\boldsymbol{P} \rightarrow$ Maximum value is $\boldsymbol{P}(1, 3) = 0.999909$.
- Search $\boldsymbol{C} \rightarrow$ '1' and '3' are in different columns
- Combine the columns '1' and '3' are in. $\rightarrow$ $m = 3 - 1 = 2$
- Set $\boldsymbol{P}(1, 3) = 0$.

Table 20. Component matrix after 4th iteration

Components Matrix, *C*				
1	0	0	4	0
3	0	0	0	0
2	0	0	0	0
5	0	0	0	0
0	0	0	0	0

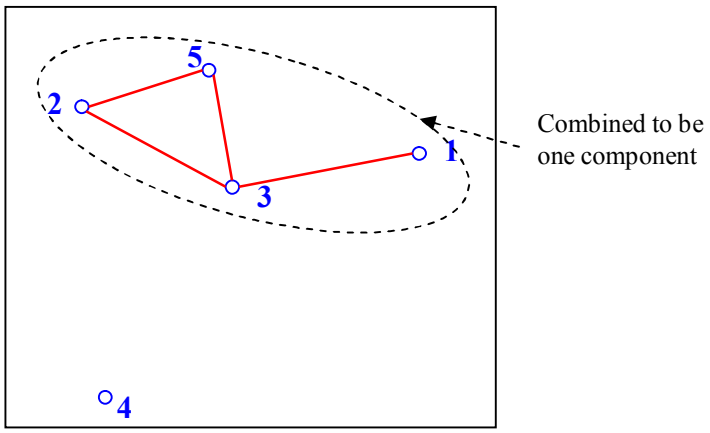

Figure 50. Graph after 4th iteration

Table 21. Connectivity probability matrix after 4th iteration

Connectivity Probability Matrix, *P*					
Node	**1**	**2**	**3**	**4**	**5**
1	1	0.029103	0	0.002468	0.991689
2	0.029103	1	0	0.559533	0
3	0.999909	0.999924	1	0.909933	0
4	0.002468	0.559533	0.909933	1	0.601714
5	0.991689	1	1	0.601714	1

Iteration 5:

- Search $\boldsymbol{P} \rightarrow$ Maximum value is $\boldsymbol{P}(1, 5) = 0.991689$.
- Search $\boldsymbol{C} \rightarrow$ '1' and '5' are in the same columns and already connected. $\rightarrow$ Go on to the next iteration.
- Set $\boldsymbol{P}(1, 5) = 0$.

Table 22. Component matrix after 5th iteration

Components Matrix, *C*				
1	0	0	4	0
3	0	0	0	0
2	0	0	0	0
5	0	0	0	0
0	0	0	0	0

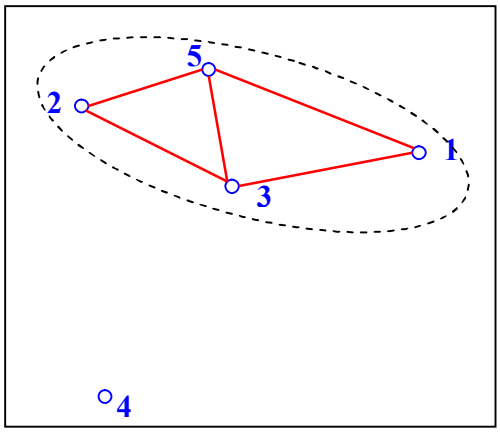

Figure 51. Graph after 5th iteration

Table 23. Connectivity probability matrix after 5th iteration

Connectivity Probability Matrix, *P*					
Node	**1**	**2**	**3**	**4**	**5**
1	1	0.029103	0	0.002468	0
2	0.029103	1	0	0.559533	0
3	0.999909	0.999924	1	0.909933	0
4	0.002468	0.559533	0.909933	1	0.601714
5	0.991689	1	1	0.601714	1

Iteration 6:

- Search $\boldsymbol{P} \rightarrow$ Maximum value is $\boldsymbol{P}(3, 4) = 0.909933$.
- Search $\boldsymbol{C} \rightarrow$ '3' and '4' are in different columns
- Combine the columns '3' and '4' are in. $\rightarrow$ $m = 2 - 1 = 1$
- Set $\boldsymbol{P}(3, 4) = 0$.
- *m=1*. Stop!

Table 24. Component matrix after 6th iteration

Components Matrix, *C*				
1	0	0	0	0
3	0	0	0	0
2	0	0	0	0
5	0	0	0	0
4	0	0	0	0

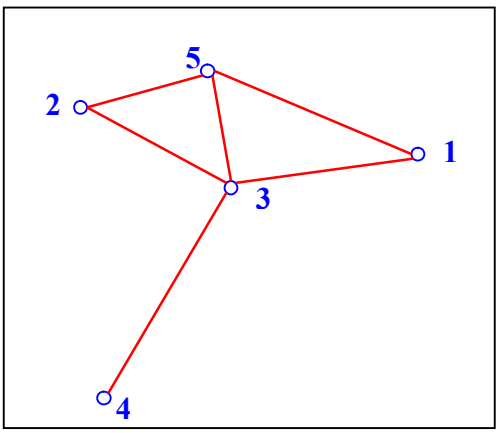

Figure 52. Graph is connected after 6th iteration.

Table 25. Connectivity probability matrix after 6th iteration

Connectivity Probability Matrix, *P*					
Node	**1**	**2**	**3**	**4**	**5**
1	1	0.029103	0	0.002468	0
2	0.029103	1	0	0.559533	0
3	0.999909	0.999924	1	0	0
4	0.002468	0.559533	0.909933	1	0.601714
5	0.991689	1	1	0.601714	1

After six iterations, the network is connected and the weakest link has been found. The weakest link to confirm $k = 1$ connectivity is $\boldsymbol{P}(3, 4) = 0.909933$.

5.4 Results and Discussion

We used modified Kruskal's algorithm to analyze connectivity within simulated networks as the following parameters were varied: path loss exponent, n; shadowing component, σ, and number of nodes deployed, N. The results of the simulations are plotted in Fig. 53-55. Each data point in figures is averaged over 10 runs.

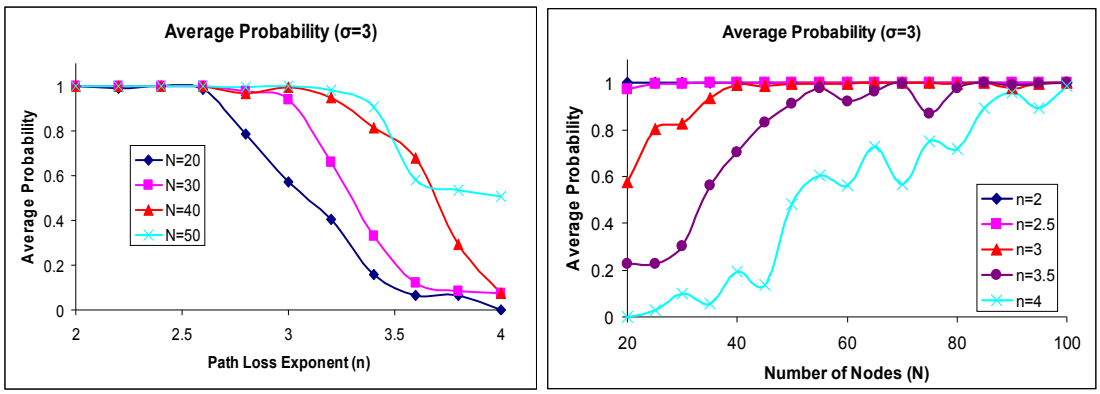

Figure 53. Average of weakest link in shadowing environments ($\sigma = 3$)

In Fig. 53, the curves in the left figure represent the influence of n on average probability based on specific N. We can see all curves in it show trend of decreasing reliability as n becomes larger. The influence of the path loss exponent to the link probabilities is to be expected, since as we know, the signal strength becomes weaker as the path loss exponent becomes large. Curves in the right figure of Fig. 53 represent the influence of N based on specific n. If we choose a specific x-value, N, curves representing

higher n, will have a larger y-value, average probability. This is caused by the influence of n, which has also been shown in the left figure. Moreover, we can see that the link reliability increases with the number of nodes. This phenomenon is caused by the fact that larger N means higher density of nodes, so they will be closer to each other on average. Thus higher link reliability can be expected in simulation results of larger N. Similar results can be found in the left figure as well. If we fix x-value in the left, curves representing larger N, resulting in higher y-value, average probability.

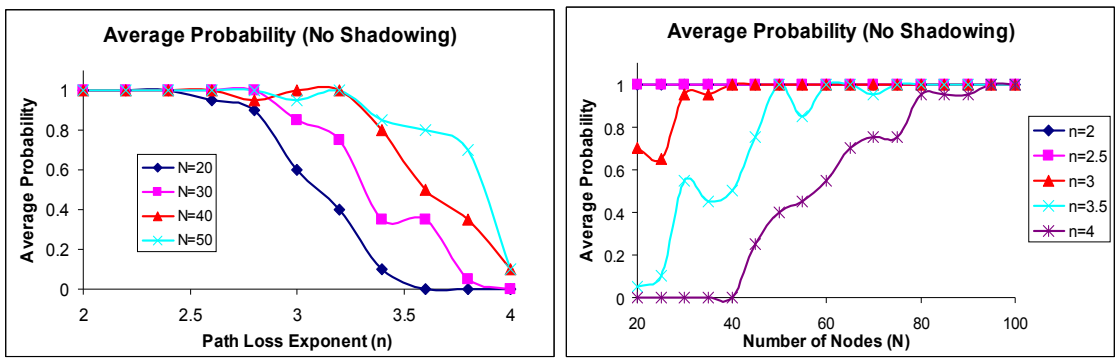

Figure 54. Average of weakest link without shadowing coefficient ($\sigma = 0$)

Fig. 54 contains the curves of average probability without shadowing coefficient. If we do not consider shadowing in the propagation environment, when the locations of nodes are fixed, the connection between each pair of nodes in the network would be either connected (100%) or disconnected (0%). So all data points of average probability in Fig. 54 are averaged over a series of 1 and 0, which consists of the results of 20 runs. If comparing the figures of Fig. 54 with their corresponding figures with shadowing coefficient, in Fig. 54, we can conclude that they have similar increasing or decreasing property. For example, both the left figure in Fig. 53 and Fig. 54 illustrate the decreasing

trend of signal as n become larger. Thus, even though the shadowing component influences the signal propagation and footprint, it does not change the influences of n, N on the link reliability.

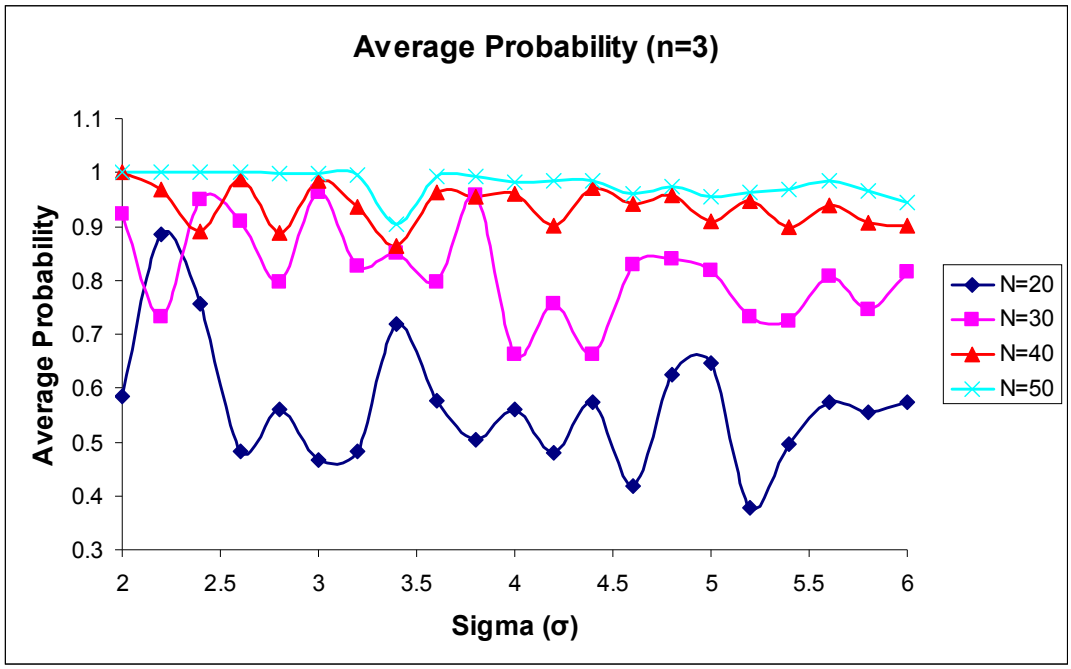

Figure 55. Average of weakest link by varying shadowing component (σ)

As the shadowing component, in Fig. 55, the curves do not have increasing or decreasing trends, but we can find out that the curves represent higher N are flatter than the lower ones. So as we expected the networks with higher node-density have consistently higher robustness, especially in highly variable environments.

5.5 Conclusion

The connectivity of random graphs was discussed in this chapter. Definitions from Graph theory are brought in to better describe the random networks. An algorithm is adapted to decide the weakest link confirming 1-connectivity of a random graph. The parameters in the algorithm (e.g. path loss exponent, n, shadowing component, σ, number of nodes, N) can be changed to simulate specific settings of networks. Using the algorithm, various network scenarios were simulated. From the results, we can find out that the probabilities of the weakest links increase (i.e., network becomes more robust) as the number of nodes increases; decrease as the path-loss exponent increases and has no obvious trend as the shadowing component changes. While the first result is intuitive, these latter two provide interesting insight that should be considered when developing a sensor network.

Clearly, these results are dependent on the specific graph configurations. In our work, attempts were made to analytically solve this problem of an arbitrary distribution of N nodes. However, this problem proved intractable. That being said an analysis of expected link distance for $N = 2$ nodes was conducted and is included in Appendix B.

CHAPTER 6

CONCLUSION

In this work, we have leveraged the W-M model to better represent the wireless communication footprints for sensor nodes. Analyses of empirical data and usability for log-normal shadowing have been presented for this model. In addition, we also analyzed the connectivity of wireless sensor networks at the system level. We conclude this thesis by reviewing the significant contributions and identifying avenues for future work.

6.1 Contributions of Work

- *'Weak-Monotonicity' model is investigated to better represent the communication footprints for wireless sensors.*

  The W-M model is viewed to be more suitable for representing practical signal footprint than the transitional disc model. This model improves upon the commonly used disc model assuming the footprint to be isotropic, which is really not the case, considering that the footprint is highly influenced by the environment, which is non-isotropic.

- *Usability of the W-M footprint is analyzed for log-normal shadowing environments.*

  Because of the fact that signal propagation is influenced by the environment, which is also non-homogeneous, even at the same T-R distance, signal power may vary. Log-normal shadowing model provides a better way to characterize the signal propagation in that this model uses a shadowing component to represent the variability of the signal power. We present in Chapter 2 an analysis of the usability which is the

percentage of the area with signal power strong enough to make reliable links. Usability analysis had been done for disc model in previous work and in this work we have introduced it for the W-M model.

- *A footprint model consisting overlapping W-M footprints is proposed.*

  W-M model is directional, so it can overcome the main shortcoming of the disc model. Moreover, in Chapter 3, we use overlapping multiple W-M footprint circles to model a more realistic contour of the real footprints in various scenarios.

- *Empirical data was collected and analyzed in context of the overlapping W-M model.*

  Three indoor scenarios were considered in Chapter 4. While the W-M model did not give a perfect way of representing the empirical data, the approach is demonstrated to be more realistic than the disc model.

- *Connectivity of randomly deployed wireless sensor networks is explored.*

  Understanding of the network connectivity can help us improve the reliability of wireless sensor networks. In order to better analyze the connectivity of wireless sensor networks, graph theory is employed in Chapter 5. Networks are described by graphs, for example, vertices represent nodes and edges represent links. Link reliability is defined to each link based on log-normal shadowing model as the probability of this link to have signal power high enough to build a reliable connection. A connectivity probability matrix is then built to represent link reliabilities between each pair of nodes. Based on this matrix, an algorithm is developed to find the highest link reliability threshold, the link with probability higher than which are considered to be connected, confirming 1-connectivity of

randomly deployed networks. Simulation results were presented which illustrate the influence of the number of nodes deployed, path-loss exponent and shadowing coefficient to the network connectivity.

6.2 Future Work

Even though the W-M model is directional and viewed herein to be better than the disc model, it still has limitations. From the empirical data we collected in Chapter 4, we find that the contour of each signal power level is not as smooth as our model. This is because of the existence of the shadowing. The shadowing contour may be like Fig. 56. So a coefficient describes the fluctuation of the signal contour might be introduced into the footprint model to represent the fluctuation of the footprint contour.

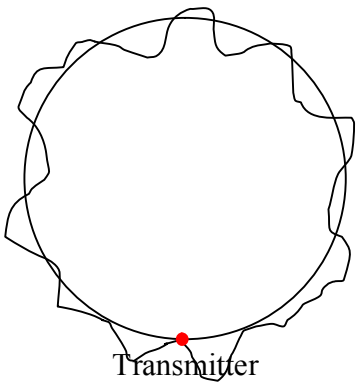

Figure 56. Signal contour

The empirical work of Chapter 4 just considered indoor settings. However, signal propagation in an outdoor area differs from indoor. For example, we might get better line

of sight and have more/fewer obstacles outdoors. More data can be collected at outdoors to evaluate the W-M modeling approach.

Also, the footprint model did not explicitly consider what type of antenna the sensor utilizes. The W-M model is clearly directional and provides a contour that may be achieved by a wall mounted patch antenna. However, sensor nodes typically utilize an omni-directional antenna and thus our empirical data did likewise. In short, work may be done to consider the antenna pattern and environmental influences on a jointly footprint.

In the connectivity analysis, the link reliabilities are built up on log-normal shadowing model and just dependent on the distance in between, general path-loss exponent and shadowing coefficient. So the link reliability is not directional. As we already discussed before, the signal propagation is directional because of the influence of non-isotropic environment. So consideration about the direction should be added into the analyses of connectivity. Moreover, all our analyses of connectivity are theoretical. Analyses of empirical networks deployed over some area can be worked on to better understand the real case. If the basic information like number and location of nodes is known for some real network, the W-M model, in conjunction with log-normal shadowing model, can be use to evaluate the connectivity prior to deployment.

Knowing the influence of the path-loss exponent, shadowing coefficient and number of nodes on the network connectivity, we can try to find a reasonable density of nodes for a wireless sensor network in order to provide a good balance between the robustness and cost according to the application and requirements of the work.

6.3 Conclusion

The W-M model provides us with a better way to represent wireless communication footprints, which is important for the analysis of wireless sensor networks. We believe that we can use overlapping W-M footprints to build more realistic footprint contour. Usability of the W-M model helps us better analyze effectiveness of communication for a sensor node. Since our theoretical and simulation results turn out to be agree with each other quite well, we can use simulation to find out the usability of some specific footprint, which is more efficient than theoretical derivative. At the network level, an algorithm has been developed to find the strongest weakest link of a randomly deployed network, which can make the network connected. We can vary the number of nodes, path-loss exponent and shadowing coefficient to set up a specific network according to what we need. We hope this work helps researchers analyze the wireless sensor networks more accurately and to design wireless sensor systems which save energy, have extended lifetime, and improved robustness.

REFERENCE

[1] G. Pei, C. Chien (2001). “Low Power TDMA in Large Wireless Sensor Networks.” Military Communications Conference, 2001, MILCOM 2001.

[2] A. Mainwarning, J. Polastre, R. Szewczyk, D. Culler, J. Anderson (2002). “Wireless Sensor Networks for Habitat Mornitoring.” Wireless Sensor Networks and Application, IPSN’02. Atlanta, Georgia, USA.

[3] R. D’Souza, D. Galvin, C. Moore, D. Randall (2006). “Global Connectivity from Local Geometric Constraints for Sensor Networks with Various Wireless Footprints.” International Conference on Information Processing in Sensor Networks, IPSN’06. Nashville, Tennessee, USA.

[4] J. Molina-Garcia-Pardo, A. Martinez-Sala, M. Bueno-Delgado, E. Egea-Lopez, L. Juan-Llacer, J. Garcia-Haro (2005). “Channel Model at 868 MHz for Wireless Sensor Networks in Outdoor Sceniarios.” International Workshop on Wireless Ad Hoc Networks, IWWAN 2005. London, UK.

[5] R. Hekmat, P. Van Mieghem (2006). "Connectivity in Wireless Ad-Hoc Networks with a Log-Normal Radio Model." Mobile Networks and Applications **11**(3): 351-360.

[6] A. Fanimokun, J. Frolik (2003). “Effects of natural propagation environments on wireless sensor network coverage area.” 2003 Southeastern Symposium on System Theory. SSST 2003.

[7] K. Sohrahi, et al (1999). “Near ground wideband channel measurement in 800-1000 MHz.” IEEE Vehicular Technology Conference, Vol. 1, July 1999, pp. 571-574.

[8] T. Rappaport, Ed. (1996). Wireless Communications, Principles and Practice, Prentice Hall PTR.

[9] M. Haenggi (2002). “Energy-balancing Strategies for Wireless Sensor Networks.” Circuits and Systems, 2003. ISCAS '03.

[10] A. Cerpa, D. Estrin (2004). "ASCENT: Adaptive Self-Configuring sEnsor Networks Topologies." IEEE Transactions on Mobile Computing **3**(3): 272-285.

[11] A. Aguiar, J. Gloss (2003). “Wireless Channel Models.” TKN Technical Reports Series. A. Wolisz. Berlin, Technical University Berlin, TKN Telecommunication Networks Group.

[12] B. Krishnamachari, Ed. (2007). Networking Wireless Sensors, Cambridge University Press.

[13] A. Wang, A. Chandrakasan (2002). "Energy-Efficient DSPs for Wireless Sensor Networks." Signal Processing Magazine, IEEE **19**(4): 68-78.

[14] M. Halgamuge, S. Guru, A. Jennings (2003). “Energy Efficient Cluster Formation in Wireless Sensor Network.” 10th International Conference on Telecommunications, 2003

[15] M. Zuniga, B. Kirshnamachari (2004). “Analyzing the transitional region in low power wireless links.” 2004 First Annual IEEE Communications Society Conference on Sensor and Ad Hoc Communications and Networks, 2004. IEEE SECON 2004. **:** 517-526.

[16] D. West, Introduction to graph theory (Second Edition), Prentice Hall 2001, 1996.

[17] “Cellular Phone Towers”. Copyright 2008 © American Cancer Society, Inc. http://www.cancer.org/docroot/PED/content/PED_1_3X_Cellular_Phone_Towers.asp

[18] J. Chen, A. Jiang, I. A. Kanj, G. Xia and F. Zhang (2007). “Separability and Topology Control of Quasi Unit Disk Graphs.” INFOCOM 2007. 26th IEEE International Conference on Computer Communications. IEEE. May 2007. Page(s):2225 – 2233.

APPENDICES

Appendix A

Connectivity Probability Matrix for Fig. 44

Node	1	2	3	4	5	6	7	8	9	10	11	12	13	14	15	16
1	+	0.031317	8E-15	1	0.315355	1.6E-05	0.999973	0.112341	1	1E-15	0.000371	0.479474	0.000222	0.999997	0.686482	0.999848
2	0.031317	+	0	0.73997	0.874972	3.6E-10	9.24E-08	1.29E-12	7.3E-06	0	5.66E-07	4.05E-11	0.000268	0.003969	1.27E-09	0.91423
3	8E-15	0	+	5.14E-11	6.27E-07	0.946356	4.45E-13	9.15E-10	0	0.847778	0.65707	2.82E-10	0.178457	1.47E-07	1.46E-08	1.09E-09
4	1	0.73997	5.14E-11	+	0.999998	0.003939	0.754212	0.009521	0.387252	7.8E-14	0.109788	0.070078	0.229924	1	0.310921	1
5	0.315355	0.874972	6.27E-07	0.999998	+	0.097199	0.001807	1.11E-05	5.74E-05	5.02E-12	0.873867	9.33E-05	0.999949	0.995409	0.003028	1
6	1.6E-05	3.6E-10	0.946356	0.003939	0.097199	+	0.000646	0.038791	1.26E-09	0.403236	1	0.028635	0.99966	0.504436	0.243099	0.014825
7	0.999973	9.24E-08	4.45E-13	0.754212	0.001807	0.000646	+	1	0.999931	1.84E-11	0.000941	1	1.86E-05	0.999409	1	0.270572
8	0.112341	1.29E-12	9.15E-10	0.009521	1.11E-05	0.038791	1	+	0.05928	2.97E-06	0.007052	1	1.51E-05	0.387599	0.241612	0.096053
9	1	7.3E-06	0	0.387252	5.74E-05	1.26E-09	0.999931	0.05928	+	0	1.36E-08	0.314497	1.92E-09	0.387599	0.241612	0.096053
10	1E-15	0	0.847778	7.8E-14	5.02E-12	0.403236	1.84E-11	2.97E-06	0	+	0.008162	2.44E-07	6.68E-06	6.65E-09	2.03E-06	2.9E-13
11	0.000371	5.66E-07	0.65707	0.109788	0.873867	1	0.000941	0.007052	1.36E-08	0.008162	+	0.00906	1	0.892537	0.134329	0.335906
12	0.479474	4.05E-11	2.82E-10	0.070078	9.33E-05	0.028635	1	1	0.314497	2.44E-07	0.00906	+	3.81E-05	0.971035	1	0.012938
13	0.000222	0.000268	0.178457	0.229924	0.999949	0.99966	1.86E-05	1.51E-05	1.92E-09	6.68E-06	1	3.81E-05	+	0.651435	0.001904	0.70827
14	0.999987	0.003969	1.47E-07	1	0.995409	0.504436	0.999605	0.797724	0.387599	6.65E-09	0.892537	0.971035	0.651435	+	0.999914	1
15	0.686482	1.27E-09	1.46E-08	0.310921	0.003028	0.243099	1	1	0.241612	2.03E-06	0.134329	1	0.001904	0.999914	+	0.113416
16	0.999848	0.91423	1.09E-09	1	1	0.014825	0.270572	0.001505	0.096053	2.9E-13	0.333906	0.012938	0.70827	1	0.113416	+
17	0.009575	2.3E-09	0.033601	0.106484	0.116747	1	0.321353	0.956746	1.16E-05	0.056776	1	0.942422	0.871797	0.99744	0.999704	0.134938
18	6.28E-08	0	0.08243	5.99E-07	7.06E-07	0.999189	0.000956	0.609628	1.52E-10	0.997947	0.57338	0.289367	0.003725	0.010761	0.549329	7.16E-07
19	0.012885	9.58E-06	0.140762	0.563927	0.988711	1	0.021945	0.05526	1.41E-06	0.001025	1	0.082542	1	0.999504	0.523607	0.838687
20	0.000126	5.25E-10	0.678028	0.011826	0.10179	1	0.006788	0.213827	2.11E-08	0.327919	1	0.170709	0.996169	0.784155	0.652009	0.030712
21	0.817076	0.999874	6.31E-10	1	1	0.002311	0.004777	4.43E-06	0.001828	1E-14	0.172285	5.86E-05	0.797227	0.991452	0.001463	1
22	0.000115	0.219011	5.53E-05	0.311495	1	0.056062	8.34E-08	1.66E-09	3.86E-10	7.4E-12	0.820162	1.08E-08	1	0.113554	9.99E-07	0.882821
23	1.23E-08	0	0.717355	5.54E-07	4.63E-06	1	5.92E-05	0.115527	7.32E-12	0.999995	0.92391	0.037234	0.044835	0.007135	0.159607	1.25E-06
24	2.9E-09	2.21E-09	0.999915	4.1E-05	0.133188	0.999917	2.39E-09	5.73E-08	1.3E-14	0.003857	1	6.19E-08	1	0.003138	4.87E-06	0.000883
25	0.004977	1E-15	3.15E-13	3.19E-05	3.08E-09	7.6E-05	0.998013	1	0.020961	2.32E-08	4.69E-06	1	2.51E-09	0.04305	0.999998	1.95E-06
26	1.19E-08	6.95E-06	0.295523	0.000485	0.76047	0.578661	2.33E-10	2.5E-10	2.1E-14	1.7E-07	0.995075	6.08E-10	1	0.00212	7.25E-08	0.013098
27	2.91E-10	0	8.37E-06	1.61E-10	9.63E-12	0.05186	0.000169	0.653596	1.43E-11	0.642841	0.000371	0.217771	4.02E-08	1.87E-05	0.204318	6.79E-11
28	0.993344	1.06E-08	0	0.039877	1.52E-07	2.21E-11	0.998437	0.049834	1	0	1.15E-10	0.245622	6.35E-12	0.036802	0.111569	0.001422
29	4.07E-07	8.15E-07	0.888718	0.003424	0.796875	0.999877	8.78E-08	4.06E-07	1.79E-12	0.000164	1	6.75E-07	1	0.056996	4.99E-05	0.04371
30	0.993616	1	1E-15	1	0.989441	1.33E-07	0.004674	1.66E-07	0.094066	0	5.17E-05	4.52E-06	0.001817	0.603538	6.12E-05	1

17	18	19	20	21	22	23	24	25	26	27	28	29	30
0.009575	6.28E-08	0.012885	0.000126	0.817076	0.000115	1.23E-08	2.9E-09	0.004977	1.19E-08	2.91E-10	0.993344	4.07E-07	0.993616
2.3E-09	0	9.58E-06	5.25E-10	0.999874	0.219011	0	2.21E-09	1E-15	6.95E-06	0	1.06E-08	8.15E-07	1
0.038601	0.08243	0.140762	0.678028	6.31E-10	5.55E-05	0.717355	0.999915	3.15E-13	0.295523	8.37E-06	0	0.888718	1E-15
0.106484	5.99E-07	0.563927	0.011826	1	0.311495	5.54E-07	4.1E-05	3.19E-05	0.000485	1.61E-10	0.039877	0.003424	1
0.116747	7.06E-07	0.988711	0.10179	1	1	4.63E-06	0.133188	3.08E-09	0.76047	9.63E-12	1.52E-07	0.796875	0.989441
1	0.999189	1	1	0.002311	0.056062	1	0.999917	7.6E-05	0.578661	0.05186	2.21E-11	0.999877	1.33E-07
0.321353	0.000956	0.021945	0.006788	0.004777	8.34E-08	5.92E-05	2.39E-09	0.998013	2.33E-10	0.000169	0.998437	8.78E-08	0.004674
0.956746	0.609628	0.05526	0.213827	4.43E-06	1.66E-09	0.115527	5.73E-08	1	2.5E-10	0.653596	0.049834	4.06E-07	1.66E-07
1.16E-05	1.52E-10	1.41E-06	2.11E-08	0.001828	3.86E-10	7.32E-12	1.3E-14	0.020961	2.1E-14	1.43E-11	1	1.79E-12	0.094066
0.056776	0.997947	0.001025	0.327919	1E-14	7.4E-12	0.999995	0.003857	2.32E-08	1.7E-07	0.642841	0	0.000164	0
1	0.57358	1	1	0.172285	0.820162	0.93391	1	4.69E-06	0.995075	0.000371	1.15E-10	1	5.17E-05
0.942422	0.289367	0.082542	0.170709	5.86E-05	1.08E-08	0.037234	6.19E-08	1	6.08E-10	0.217771	0.245622	6.75E-07	4.52E-06
0.871797	0.003725	1	0.996169	0.797227	1	0.044835	1	2.51E-09	1	4.02E-08	6.35E-12	1	0.001817
0.99744	0.010761	0.999504	0.784155	0.991452	0.113554	0.007135	0.003138	0.04305	0.00212	1.87E-05	0.036802	0.056996	0.605338
0.999704	0.549329	0.523607	0.652009	0.001463	9.99E-07	0.159607	4.87E-06	0.999998	7.25E-08	0.204518	0.111569	4.99E-05	6.12E-05
0.134938	7.16E-07	0.838687	0.030712	1	0.882821	1.25E-06	0.000883	1.95E-06	0.013098	6.79E-11	0.001422	0.04371	1
\	0.999992	1	1	0.009537	0.005523	0.999995	0.42116	0.111209	0.018285	0.418596	5.09E-07	0.60887	6.45E-06
0.999992	\	0.508179	0.999976	7.93E-09	2.53E-08	1	0.011557	0.068211	4.33E-06	1	2.25E-11	0.004864	8.29E-13
1	0.508179	\	1	0.546898	0.851253	0.821771	0.998925	7.98E-05	0.928845	0.000459	1.38E-08	0.999999	0.001328
1	0.999976	1	\	0.003428	0.027433	1	0.988743	0.001217	0.268533	0.159105	4.9E-10	0.992667	3.92E-07
0.009537	7.93E-09	0.546898	0.003428	\	0.999337	3.04E-08	0.001497	1.95E-09	0.070335	2.05E-13	6.47E-06	0.075067	1
0.005523	2.53E-08	0.851253	0.027433	0.999337	\	7.47E-07	0.788367	1.6E-13	1	5.6E-14	5.04E-13	0.999152	0.095541
0.999995	1	0.821771	1	3.04E-08	7.47E-07	\	0.222552	0.001887	0.000305	0.995849	5.52E-13	0.093298	1.16E-12
0.42116	0.011557	0.998925	0.988743	0.001497	0.788367	0.222552	\	7.66E-12	1	1.05E-07	0	1	1.3E-08
0.111209	0.068211	7.98E-05	0.001217	1.95E-09	1.6E-13	0.001887	7.66E-12	\	1.9E-14	0.432584	0.054497	5.11E-11	2.31E-10
0.018285	4.33E-06	0.928845	0.268533	0.070335	1	0.000305	1	1.9E-14	\	5.98E-12	0	1	3.48E-06
0.418596	1	0.000459	0.159105	2.05E-13	5.6E-14	0.995849	1.05E-07	0.432584	5.98E-12	\	1.17E-11	3.45E-08	0
5.09E-07	2.25E-11	1.38E-08	4.9E-10	6.47E-06	5.04E-13	5.52E-13	0	0.054497	0	1.17E-11	\	6E-15	0.001071
0.60887	0.004864	0.999999	0.992667	0.075067	0.999152	0.093298	1	5.11E-11	1	3.45E-08	6E-15	\	3.98E-06
6.45E-06	8.29E-13	0.001328	3.92E-07	1	0.095541	1.16E-12	1.3E-08	2.31E-10	3.48E-06	0	0.001071	3.98E-06	\

Appendix B

Derivation of Average Distance between Two Nodes Randomly Deployed in a Unit Square

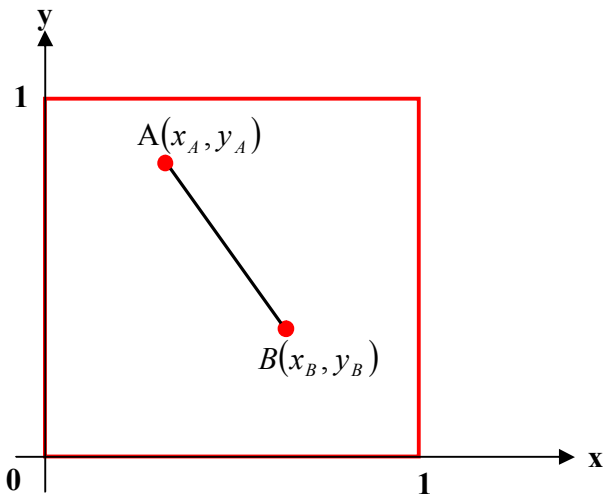

Figure 57. Distance between two nodes in a unit square.

In Fig. 57, A and B are any two randomly deployed nodes. The coordinates of them are $\mathrm{A}(x_A, y_A)$ and $B(x_B, y_B)$, where x_A, y_A, x_B, y_B are random variables uniformly distributed over $[0,1]$. The distance between these two points is:

$$D(AB) = \sqrt{(x_A - x_B)^2 + (y_A - y_B)^2} \tag{B.1}$$

The average distance between two randomly deployed nodes is the expected value of $D(AB)$.

So $$E[D(AB)] = E\left[\sqrt{(x_A - x_B)^2 + (y_A - y_B)^2}\right] \tag{B.2}$$

Since all random variables here are uniform distributed over $[0,1]$ and probability density function of uniform distribution is $f(x)=1$, we can calculate

$$E[x_A]=E[x_B]=E[y_A]=E[y_B]=\int_0^1 x\cdot f(x)\cdot dx=\int_0^1 x\cdot dx=\frac{1}{2}x^2\Big|_0^1=\frac{1}{2} \tag{B.3}$$

$$E[x_A^2]=E[x_B^2]=E[y_A^2]=E[y_B^2]=\int_0^1 x^2\cdot f(x)\cdot dx=\int_0^1 x^2\cdot dx=\frac{1}{3}x^3\Big|_0^1=\frac{1}{3} \tag{B.4}$$

Considering that x_A, y_A, x_B, y_B are mutually independent random variables,

$$E[x_Ax_B]=E[x_A]\cdot E[x_B]=\frac{1}{4};\qquad E[y_Ay_B]=E[y_A]\cdot E[y_B]=\frac{1}{4}.$$

So we get

$$\begin{aligned}&E[(x_A-x_B)^2+(y_A-y_B)^2]\\&=E[x_A^2+x_B^2-2x_Ax_B+y_A^2+y_B^2-2y_Ay_B]\\&=E[x_A^2]+E[x_B^2]-2E[x_A]E[x_B]+E[y_A^2]+E[y_B^2]-2E[y_A]E[y_B]\end{aligned} \tag{B.5}$$

Bring the values of equs. (B.3) and (B.4) into equ. (B.5),

$$E[(x_A-x_B)^2+(y_A-y_B)^2]=\frac{1}{3}+\frac{1}{3}-2\times\frac{1}{2}\times\frac{1}{2}+\frac{1}{3}+\frac{1}{3}-2\times\frac{1}{2}\times\frac{1}{2}=\frac{1}{3}$$

So $$E\left[\sqrt{(x_A-x_B)^2+(y_A-y_B)^2}\right]=\sqrt{\frac{1}{3}}=\frac{\sqrt{3}}{3}\approx 0.577$$

Thus the average distance between two nodes randomly deployed within a unit square is about 0.577.